

AFRL-VA-WP-TR-2002-3005

**DEVELOPMENT OF VALIDATED CRACK
MEASUREMENT SYSTEM FOR
VIBRATING STRUCTURES**

MOHAN M. RATWANI, PH.D

**R-TEC
28441 HIGHRIDGE ROAD
SUITE 530
ROLLING HILLS ESTATES, CA 90274**



JANUARY 2002

FINAL REPORT FOR PERIOD OF 10 APRIL 2001 – 09 JANUARY 2002

THIS IS A SMALL BUSINESS INNOVATION RESEARCH (SBIR) PHASE 1 REPORT

Approved for public release; distribution unlimited.

20020315 054

**AIR VEHICLES DIRECTORATE
AIR FORCE RESEARCH LABORATORY
AIR FORCE MATERIEL COMMAND
WRIGHT-PATTERSON AIR FORCE BASE, OH 45433-7542**

REPORT DOCUMENTATION PAGE

Form Approved
OMB No. 074-0188

Public reporting burden for this collection of information is estimated to average 1 hour per response, including the time for reviewing instructions, searching existing data sources, gathering and maintaining the data needed, and completing and reviewing this collection of information. Send comments regarding this burden estimate or any other aspect of this collection of information, including suggestions for reducing this burden to Washington Headquarters Services, Directorate for Information Operations and Reports, 1215 Jefferson Davis Highway, Suite 1204, Arlington, VA 22202-4302, and to the Office of Management and Budget, Paperwork Reduction Project (0704-0188), Washington, DC 20503

| | | |
|---|---------------------------------------|---|
| 1. AGENCY USE ONLY (Leave blank) | 2. REPORT DATE JANUARY 2002 | 3. REPORT TYPE AND DATES COVERED Final, 04/10/2001 – 01/09/2002 |
|---|---------------------------------------|---|

| | |
|--|--|
| 4. TITLE AND SUBTITLE DEVELOPMENT OF VALIDATED CRACK MEASUREMENT SYSTEM FOR VIBRATING STRUCTURES | 5. FUNDING NUMBERS C: F33615-01-M-3127 PE: 65502F PR: 3005 TA: 42 WU: 27 |
|--|--|

| | |
|---|--|
| 6. AUTHOR(S) MOHAN M. RATWANI, PH.D | |
|---|--|

| | |
|--|---|
| 7. PERFORMING ORGANIZATION NAME(S) AND ADDRESS(ES) R-TEC 28441 HIGHRIDGE ROAD SUITE 530 ROLLING HILLS ESTATES, CA 90274 | 8. PERFORMING ORGANIZATION REPORT NUMBER R-Tec 02-1 |
|--|---|

| | |
|--|--|
| 9. SPONSORING / MONITORING AGENCY NAME(S) AND ADDRESS(ES) AIR VEHICLES DIRECTORATE AIR FORCE RESEARCH LABORATORY AIR FORCE MATERIEL COMMAND WRIGHT-PATTERSON AIR FORCE BASE, OH 45433-7542 POC: David Banaszak, AFRL/VASM, (937) 255-6104 x354 | 10. SPONSORING / MONITORING AGENCY REPORT NUMBER AFRL-VA-WP-TR-2002-3005 |
|--|--|

| |
|--|
| 11. SUPPLEMENTARY NOTES THIS IS A SMALL BUSINESS INNOVATION RESEARCH (SBIR) PHASE 1 REPORT |
|--|

| | |
|---|-------------------------------|
| 12a. DISTRIBUTION / AVAILABILITY STATEMENT Approved for public release; distribution unlimited. | 12b. DISTRIBUTION CODE |
|---|-------------------------------|

| |
|---|
| 13. ABSTRACT (Maximum 200 Words) Analyses were developed to obtain resonant frequencies of panels with and without cracks and subjected to vibratory loads. These analyses were extended to panels with bonded composite patches. A dynamic stress analysis method was developed for panels tested under vibratory loads produced by shaker excitation. Analytically predicted resonant frequencies and stresses compared well with test data provided by Wright Patterson Air Force Base (WPAFB). A review of crack growth data, obtained at WPAFB under vibratory loads, indicated that conventional stress intensity factor (SIF) solutions in AFGROW or other crack growth codes could not be used for accurate prediction of crack growth because of absence of methodology accounting for dynamic stresses and frequency effects. The SIF used in AFGROW were modified to account for these factors. Using the modified SIF, crack growth predictions were made for the WPAFB data on panels with and without bonded composite patches. A good correlation was obtained between predictions and test data. A Visual Crack Measurement System (VCMS) was used to monitor cracks in the WPAFB tests. An integrated VCMS design was developed. The integrated VCMS will perform crack measurement and structural integrity evaluation functions. The integrated system will also design repair patches for dynamic loading. |
|---|

| | |
|--|--------------------------------------|
| 14. SUBJECT TERMS Acoustic Fatigue, AFGROW Code, Crack Growth, Composite Patches, Resonant Frequencies, Visual Crack Measurement System, Vibratory Loads | 15. NUMBER OF PAGES 42 |
|--|--------------------------------------|

| | |
|--|-----------------------|
| | 16. PRICE CODE |
|--|-----------------------|

| | | | |
|--|---|--|--|
| 17. SECURITY CLASSIFICATION OF REPORT Unclassified | 18. SECURITY CLASSIFICATION OF THIS PAGE Unclassified | 19. SECURITY CLASSIFICATION OF ABSTRACT Unclassified | 20. LIMITATION OF ABSTRACT SAR |
|--|---|--|--|

| | | |
|----------------------|--|--|
| NSN 7540-01-280-5500 | | Standard Form 298 (Rev. 2-89) Prescribed by ANSI Std. Z39-18 298-102 |
|----------------------|--|--|

PROJECT SUMMARY

AIR FORCE SBIR- PHASE I FINAL REPORT

TOPIC Number AF01-240

Contract No.: F33615-01-M-3127

PROJECT TITLE: Development of Validated Crack Measurement System for Vibrating Structures

COMPANY: R-Tec

ADDRESS: 28441 Highridge Road, Suite 530
Rolling Hills Estates, California 90274

SUMMARY:

Maintaining the airworthiness of aircraft is of prime concern to manufacturers, operators and regulatory authorities. In-service failure prevention is an integral part of an aircraft structural integrity program. Thin-skinned aircraft structures in high-intensity acoustic environments are prone to develop cracks in the skins, often at joints to substructure. Such cracks are referred to as acoustic fatigue cracks. It is desirable to know the rate of acoustic fatigue crack growth until the crack reaches a critical length and poses a realistic threat to aircraft safety. A knowledge of the crack growth rate and the critical length is useful information in establishing inspection requirements for the cracks and determining whether or not an aircraft can safely make additional flights in a warfare emergency before a repair is performed. Although generally acceptable methods exist for predicting the onset of fatigue cracks caused by acoustic loading, there are no acceptable methods for predicting the growth of such cracks (and their critical lengths) which may cause the catastrophic loss of the aircraft under certain flight conditions.

The Wright-Patterson Air Force Base has generated a comprehensive fatigue test database on aluminum panels subjected to shaker excitation. A Visual Crack Measurement System (VCMS) was used to monitor cracks in the tests. These data were provided by the Air Force to R-Tec for analysis verification. A systematic step-by-step approach was used to develop analyses and then verify with the test data. Analyses were developed to obtain resonant frequencies of panels with and without cracks and subjected to vibratory loads. These techniques were extended to panels with bonded composite patches. Techniques were also developed to obtain dynamic stresses in panels tested under vibratory loads produced by shaker excitation. Analytically predicted resonant frequencies and stresses compared well with test results.

A careful review of crack growth data indicated that present stress intensity factors (SIFs) solutions in AFGROW or other crack growth codes could not be used due to the absence of methodology accounting for dynamic stresses and frequency effects. The SIFs solutions in AFGROW were modified to account for the dynamic effects. Using the modified SIFs in AFGROW, crack growth predictions were made for the Air Force provided data. A good correlation was obtained between analytical predictions and test data.

New functions to be performed by an integrated VCMS were established. The integrated VCMS will perform crack measurement as well as structural integrity evaluation functions. In addition to these functions, the system will design repair patches for dynamic loading. Requirements of the integrated VCMS and modules have been established.

SUBMITTED BY:

Date: January 9, 2002

(Mohan M. Ratwani, Ph.D., Principal Investigator)

Development of Validated Crack Measurement System for Vibrating Structures

TABLE OF CONTENTS

| Section | Page |
|---|------|
| 1. INTRODUCTION | 3 |
| 1.1 General Background | 3 |
| 1.2 Program Objective | 3 |
| 1.3 Program Approach | 4 |
| 2. ANALYTICAL DEVELOPMENT AND CORRELATION WITH TEST DATA | 5 |
| 2.1 Analytical Predictions of Resonant Frequencies | 5 |
| 2.1.1 Resonant Frequencies of Panels Without Bonded Patches | 5 |
| 2.1.2 Resonant Frequencies of Panels With Bonded Patches | 10 |
| 2.2 Dynamic Stress Analysis of Vibrating Panels and Verification with Test Data | 12 |
| 2.2.1 Dynamic Stress Analysis | 12 |
| 2.2.2 Comparison Between Predictions and Test Data | 14 |
| 2.2.3 Comparison Between Dynamic and Static Deflection Curves | 15 |
| 2.3 Damping Ratio ζ Computations from Magnification Factor | 15 |
| 3. CRACK GROWTH UNDER VIBRATORY LOADS | 17 |
| 3.1 Review of Fatigue Crack Growth Data | 17 |
| 3.1.1 Fatigue Crack Growth Behavior Including Crack Initiation | 17 |
| 3.1.2 Fatigue Crack Growth Behavior After First Crack Detection | 19 |
| 3.1.3 Comparison of Fatigue Crack Growth Behavior in Test Specimens | 22 |
| 3.2 Crack Growth Prediction | 24 |
| 3.2.1 Crack Growth Prediction in Panels Without Composite Patch | 25 |
| 3.2.2 Crack Growth Prediction in Panels With Bonded Composite Patch | 26 |
| 3.3 Assessment of AFGROW Code Capabilities | 28 |
| 4. VISUAL CRACK MEASUREMENT SYSTEM (VCMS) DEVELOPMENT | 29 |
| 5. SUMMARY AND ASSESSMENT OF TECHNICAL MERIT | 33 |
| 5.1 Summary | 33 |
| 5.2 Assessment of Technical Merit | 34 |
| 6. REFERENCES | 35 |

SECTION 1

INTRODUCTION

1.1 General Background

Maintaining the airworthiness of aircraft is of prime concern to manufacturers, operators and regulatory authorities. In-service failure prevention is an integral part of an aircraft structural integrity program. In spite of conservatism in design and verification testing, in-service failures are known to occur in aircraft structural components due to vibratory loads. In the context of present studies, a vibratory load on an aircraft structure or on a test specimen may be due to acoustic excitation, rotating equipment mounted on a structure, shaker excitation, etc. Structural design and test engineers are constantly striving to develop techniques to 1) measure damage growth due to vibratory loads, 2) predict the growth of damage in a structure under vibratory loads, 3) predict subsequent life of structural components, and 4) prevent the initiation and propagation of damage. Recent advances in crack growth measurement techniques (e.g., References 1-3) such as Visual Crack Measurement System (VCMS) has provided opportunity to develop a unified system for measuring crack growth in complex structures under harmonic and random vibratory loads.

Analytical prediction of crack initiation and growth due to vibratory loads has always been a problem due to the complex nature of the loads and state of stress produced by the loads at the damage initiation sites. Past emphasis has been primarily on tests. This is often time-consuming and expensive. Recent advances in crack initiation and growth prediction methodology and software (e.g., AFGROW, NASGROW computer programs) have provided opportunities for analytical prediction of damage initiation and growth under vibratory loads. While the analytical techniques incorporated in AFGROW or NASGROW may not be directly applicable to life prediction under vibratory loads, they provide an excellent basis for developing analytical techniques for predicting damage initiation and growth under vibratory loads.

Recent advances in the concept of repairing cracked metallic structures with composites (References 4-10) have provided new opportunities to apply this concept to: 1) Prevent acoustic fatigue failures from initiating during the life of an aircraft, and 2) Retard the growth of the cracks that have already initiated. Some of the recent studies have shown that bonding of a fiberglass reinforcement (Reference 4) can enhance the fatigue life of metallic components subjected to vibratory loads. The enhancement in fatigue life due to bonding of composite reinforcements could occur due to two reasons namely- 1) an increase in stiffness and thereby decrease in stress response and increase in fatigue life, and 2) a retardation in crack initiation and growth of cracks due to load transfer to composite patch at crack initiation sites.

Thus, there is a need to: 1) Evaluate the capability of current analytical techniques to reliably predict the initiation and growth of cracks due to vibratory loads in structures with and without composite patches, 2) Develop reliable experimental techniques to measure crack initiation and growth in structures due to vibratory loads, 3) Develop a systematic approach that needs to be followed for analytical prediction of damage initiation and growth due to vibratory loads, and 4) Develop and verify techniques to prevent/retard initiation and growth of damage due to vibratory loads.

1.2 Program Objective

The overall objective of the proposed program is to develop analytical and test procedures for reliable prediction of fatigue behavior of aircraft structures subjected to vibratory loads. The Phase I objectives of the proposed program are to: 1) Develop an integrated Visual Crack Measurement System (VCMS) for structures subjected to vibratory loads, 2) Evaluate the capabilities of present analyses and software to predict crack initiation and growth in structures subjected to vibratory loads, and 3) Evaluate the

application of current bonded repair analytical techniques to predict crack growth in structures with bonded repairs and subjected to vibratory loads.

1.3 Program Approach

Phase I program is to evaluate the capabilities of current experimental and analytical techniques to reliably predict crack initiation and growth in structures subjected to acoustic and other vibratory loads. Overall program approach is shown in Figure 1.1. Phase I effort consisted of the following five Tasks-

Task 1- Analyze Existing Test Data

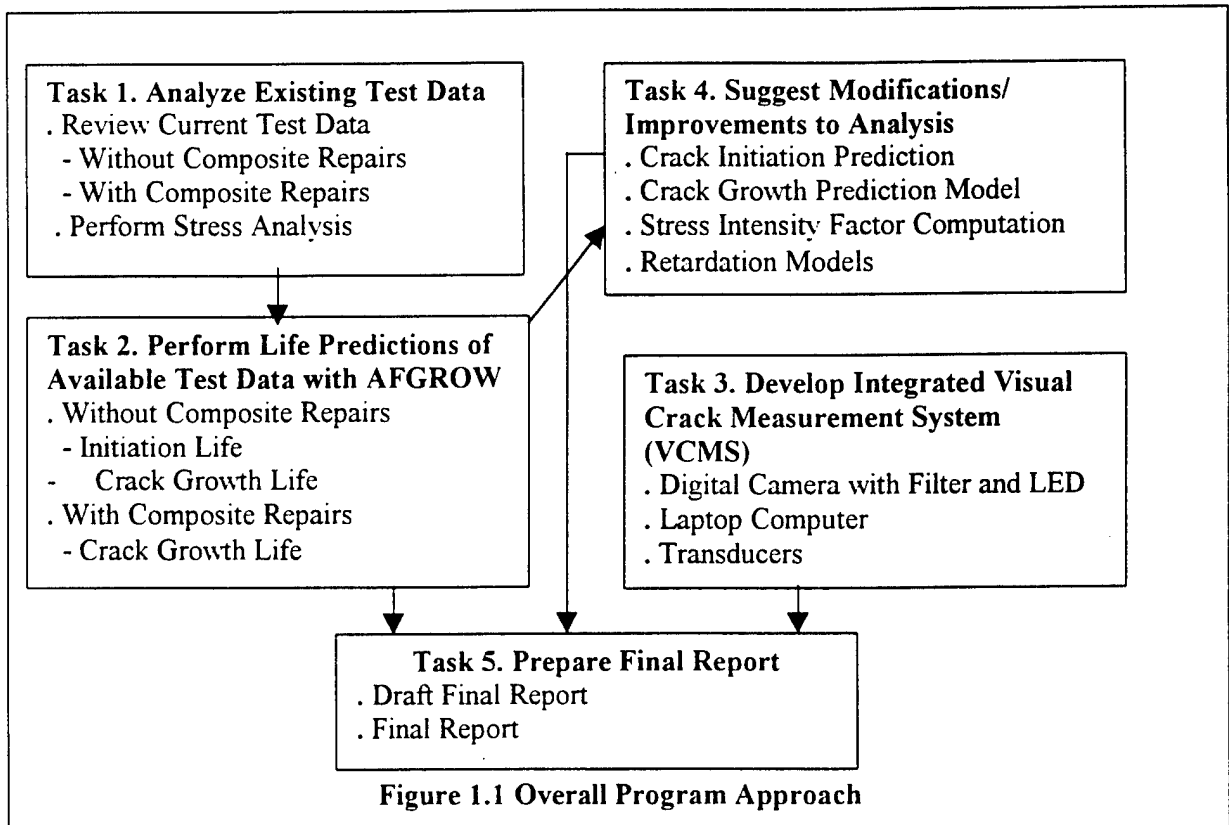
Task 2- Perform Life Predictions of Available Test Data with AFGROW

Task 3- Develop Integrated Visual Crack Measurement System (VCMS)

Task 4- Suggest Modifications/Improvements to Analysis

Task 5- Prepare Final Report

A detailed literature search was conducted to find fatigue crack growth test data under vibratory and acoustic loads. It was found that while significant data is available on fatigue life, very little information is available on crack growth data. The only meaningful test data for correlation with crack growth analysis was generated at AFRL, Wright Patterson Air Force Base (References 1-4). These data have been generated on test specimens with and without composite patches under vibratory loads produced by shaker excitation. Details of the test data were provided by the Air Force to R-Tec for evaluation. Phase I effort was concentrated on developing dynamic stress and crack growth analyses for available test data configurations. In addition, the requirements and various modules of VCMS were identified.



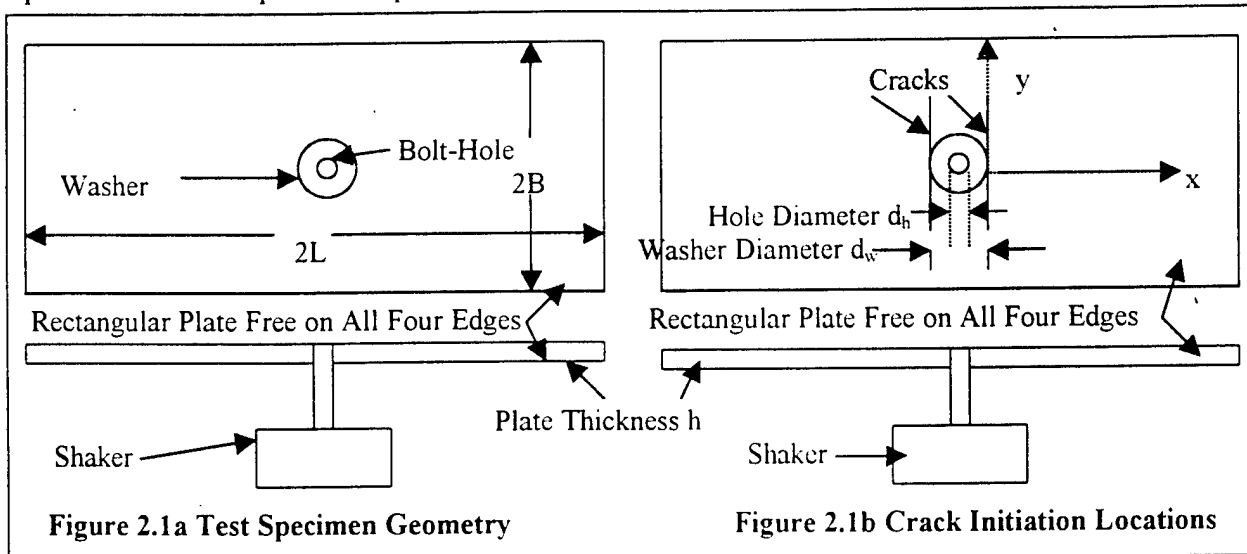
SECTION 2

ANALYTICAL DEVELOPMENT AND CORRELATION WITH TEST DATA

Fatigue and crack growth behavior prediction of structures subjected to acoustic and vibratory loads requires computation of stresses produced by the structural loading conditions. Static stress analysis does not give correct information regarding the stresses that can be used in existing fatigue and crack growth methodology. In addition, the high frequencies encountered in acoustic and vibratory loads affect the fatigue life and crack growth. Thus, a first step in developing any life prediction methodology is to have proper dynamic stress analysis. Analyses to predict resonant frequencies and stresses in structures subjected to vibratory loads are developed and correlated with available test data. The details of analyses and correlation with tests are discussed in the following paragraphs.

2.1 Analytical Predictions of Resonant Frequencies

Analytical techniques have been developed to predict resonant frequencies of panels with and without bonded patches, tested at WPAFB under vibratory loads (References 1-4). Specimen configuration shown in Figure 2.1a was tested under vibratory loads in a shaker at resonant frequencies. It was observed that resonant frequencies decreased as cracks initiated and propagated (Figure 2.1b). After cracks were grown to certain lengths, the test specimens were bonded with composite patches and testing continued. The tests indicated that the resonant frequencies of test specimens increased after bonding patches. As testing of bonded panels continued, resonant frequencies decreased with crack growth. Thus, it is necessary to predict resonant frequencies of panels with and without cracks before and after patch bonding.



2.1.1 Resonant Frequencies of Panels Without Bonded Patches

Analytical Prediction of Frequencies Before Crack Initiation

Analytical prediction of resonant frequencies for the test specimen configuration shown in Figure 2.1a was carried out for the case before cracks initiate in the specimens. The test data have shown that cracks do not initiate at the holes but away from the holes close to the washer as shown in Figure 2.1b. The vibratory motion of the plate and initiation of cracks indicates that the plate vibrates with fixity along y -axis like a cantilever beam. For analysis, the vibratory motion of the plate may be considered as bending of a cantilever beam. Bending vibrations of cantilever beams are discussed in Reference 11 based on linear theory. The first mode resonance frequency is given by:

$$\omega_0 = (1.875)^2 (EI/mL^4)^{1/2} \quad (1)$$

Where,

ω_0 = First mode resonant frequency (in radians per second)

E = Young's Modulus

I = Moment of inertia of the beam

L = Span of the beam

m = Mass per unit length

Equation 1 was used to obtain the fundamental mode frequencies for the specimens tested in References 1-4. The specimen dimensions given in the references were used in Equation 1 and are shown in Figure 2.2. The value of L in Equation 1 was taken as the distance between free edge and midway between hole-edge and washer edge as the exact fixity location in the specimens is not known. Thus, in Figure 2.1b the effective $L_{\text{effective}}$ for computing frequency is $[L - (d_h + d_w)/4]$. The values of first mode resonant frequency f_0 computed from Equation 1 for various test specimens are shown in Figure 2.2 along with the effective length used in the computations. The figure also shows test resonant frequencies. The figure shows excellent agreement between test results and analytical predictions. The excellent agreement between linear theory and test results implies that linear theory is good for predicting resonance frequencies.

| Specimen Series | Width (mm) | Length (mm) | Thickness (mm) | Effective Length(mm) | Predicted Frequency(Hz) | Test Frequency(Hz) | Percentage Difference (Average Based) |
|-----------------|------------|-------------|----------------|----------------------|-------------------------|--------------------|---------------------------------------|
| 1 | 85 | 180 | 1 | 85.7 | 111.6 | 110-112 | 0.5 |
| 2 | 85 | 180 | 3.2 | 85.7 | 348.0 | 330-336 | 4.3 |
| 3 | 170 | 360 | 1 | 175.6 | 26.6 | 27-28 | 3.3 |
| 4 | 170 | 360 | 3.2 | 175.6 | 83.0 | 82-83 | 0.6 |

Figure 2.2 Predicted and Observed Resonant Frequencies Before Crack Initiation

Analytical Prediction of Frequencies After Crack Initiation

It was observed in Reference 1-4 tests that resonant frequencies dropped as the cracks propagated in the test specimens. The results are not surprising as the stiffness of plate changes with crack growth. A simplified analysis was developed to account for the changes in resonant frequencies due to the presence of cracks. Consider the plate shown in Figure 2.3 with cracks and subjected to vibratory loads. The effective width of the plate resisting bending at support locations about which bending occurs is taken as the width of the plate minus crack length. It is assumed that the cracked portion of the plate is not effective in resisting bending and the load of the plate is taken by the effective width. In test specimens, the crack lengths will not be the same on both sides of the bolt-hole as shown in Figure 2.3. For the purposes of analysis, average crack length $(a_1 + a_2)$ is assumed. Thus the effective width of the plate resisting bending is-

$$2B - (a_1 + a_2) \quad (2)$$

Equation 1 is used to compute resonant frequencies. However, in Equation 1 effective width of $(2B - a_1 - a_2)$ is used for computing moment of inertia. In the equation, the mass m is taken for the entire width of the plate. Equation 1 for a cracked plate reduces to

$$\omega_{0c} = (1.875)^2 \{Eh^2[2B - (a_1 + a_2)] / (2B\gamma L^4)\}^{1/2} \quad (3)$$

where,

ω_{0c} = Resonant frequency with crack

γ = mass per unit volume of plate material

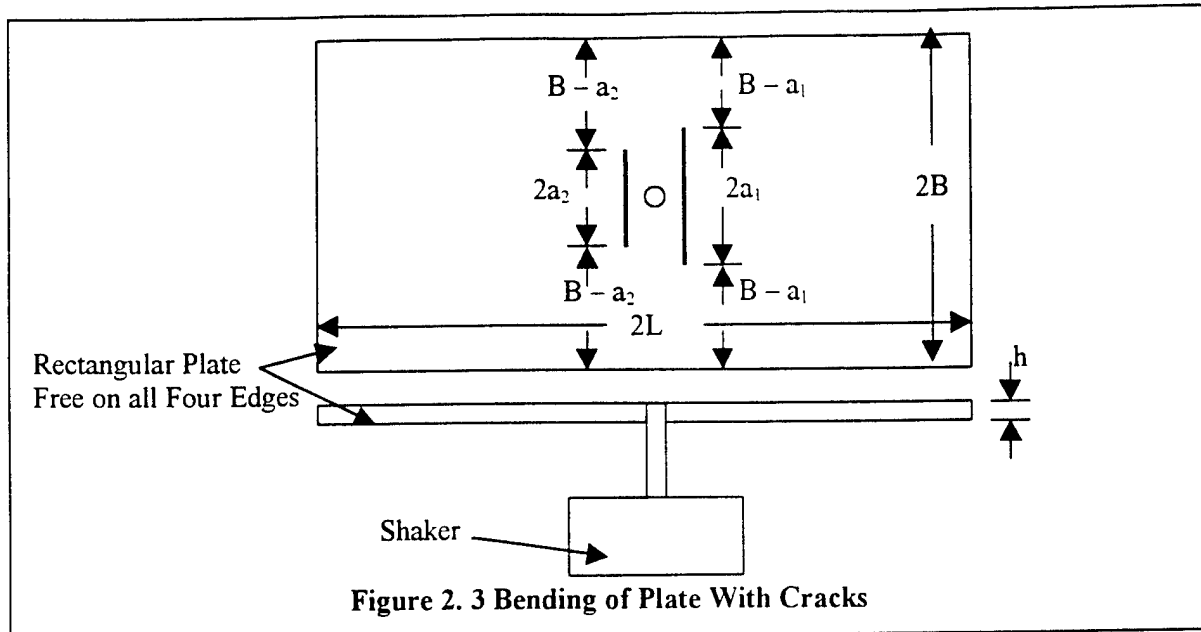
2B = Plate width

h = Plate thickness

L = Effective span of the beam

The ratio between frequencies for cracked plate and uncracked plate is given by-

$$\omega_{0c} / \omega_0 = [(2B - a_1 - a_2)/2B]^{1/2} \quad (4)$$



Equation 3 was used to compute resonant frequencies for various specimens tested at WPAFB (References 1-4). The resonant frequencies changed as cracks initiated and propagated. Predicted and observed frequencies for 85x180 x1 mm specimens without bonded repairs are shown in Figures 2.4. The figure shows a good agreement (within 6%) between predictions and test frequencies up to 40-mm crack lengths. For larger crack lengths the agreement is not good because the net section resisting bending in the 85-mm wide plate is small and the load in the cracked region causes transverse bending. The transverse bending will not result in pure one-degree-of-freedom vibrations.

| Specimen ID | Test Frequency No Crack | Crack 1 (mm) | Crack 2 (mm) | Average Crack Length(mm) | Predicted Frequency | Test Frequency With Crack | Percentage Difference |
|-----------------------|-------------------------|--------------|--------------|--------------------------|---------------------|---------------------------|-----------------------|
| TSP1 (1 mm Thickness) | | | | | | | |
| 01 | 111 | 24.9 | 25.8 | 25.35 | 93.5 | 96 | -2.6 |
| 1A | 110 | 26.6 | 21.4 | 24.00 | 94.5 | 98 | -3.6 |
| 1B | 110 | 65.6 | 64.7 | 65.15 | 54.0 | 64 | -15.6 |
| 1C | 110 | 27.3 | 23.6 | 25.45 | 93.3 | 98 | -4.8 |
| 1D | 108 | 31.2 | 30.3 | 30.75 | 89.1 | 93 | -4.2 |
| 1D | 108 | 35.9 | 35.5 | 35.70 | 85.0 | 90 | -5.5 |
| 1D | 108 | 41.8 | 39.2 | 40.50 | 80.7 | 85 | -5.0 |
| 1D | 108 | 56.7 | 55.8 | 56.25 | 64.9 | 72 | -9.8 |
| 1D | 108 | 61.0 | 63.0 | 62.0 | 58.0 | 65 | -10.7 |
| 1D | 108 | 63.6 | 70.6 | 67.1 | 51.2 | 60 | -14.6 |
| 1D | 108 | 66.9 | 74.2 | 70.55 | 46.0 | 56 | -17.8 |
| 1E | 111 | 24.9 | 24.7 | 24.8 | 93.9 | 99 | -5.2 |
| 1E | 111 | 26.3 | 26.5 | 26.4 | 92.6 | 97 | -4.5 |

Figure 2.4 Predicted and Observed Resonant Frequencies at Various Crack Lengths in 85x180x1 mm Specimens Without Bonded Patches

Predicted and observed frequencies for 85x180 mm specimens having 3.2-mm thickness without bonded repairs are shown in Figures 2.5. The predicted frequencies are within 10% of test frequencies. The percentage differences between predicted and test frequencies increase as crack length increases.

| Specimen I D | Test Frequency No Crack | Crack 1 (mm) | Crack 2 (mm) | Average Crack Length(mm) | Predicted Frequency | Test Frequency With Crack | Percentage Difference |
|------------------------------|-------------------------|--------------|--------------|--------------------------|---------------------|---------------------------|-----------------------|
| TSP2 (3 mm Thickness) | | | | | | | |
| 20 | 333 | 14.7 | 8.0 | 11.35 | 324 | 319 | +1.5 |
| 20 | 333 | 19.7 | 8.7 | 14.20 | 318 | 314 | +1.2 |
| 20 | 333 | 26.8 | 12.3 | 19.55 | 305 | 310 | -1.6 |
| 2A | 330 | 17.0 | 10.4 | 13.70 | 319 | 310 | +2.9 |
| 2A | 330 | 19.2 | 10.4 | 14.8 | 316 | 307 | +3.0 |
| 2A | 330 | 22.0 | 10.4 | 16.2 | 313 | 302 | +3.6 |
| 2A | 330 | 26.1 | 10.4 | 18.25 | 308 | 291 | +5.8 |
| 2B | 334 | 14.9 | 9.1 | 12.0 | 322 | 322 | 0 |
| 2B | 334 | 15.8 | 9.1 | 12.45 | 321 | 319 | +0.6 |
| 2B | 334 | 24.2 | 9.1 | 16.65 | 312 | 316 | -1.3 |
| 2B | 334 | 26.6 | 9.1 | 17.85 | 309 | 312 | -1.0 |
| 2B | 334 | 32.0 | 12.3 | 22.15 | 299 | 306 | -2.3 |
| 2B | 334 | 35.3 | 12.8 | 24.05 | 295 | 298 | -1.0 |
| 2B | 334 | 38.3 | 12.8 | 25.55 | 291 | 294 | -1.0 |
| 2B | 334 | 46.1 | 13.0 | 31.38 | 276 | 288 | -4.2 |
| 2C | 336 | 12.5 | 12.7 | 12.60 | 321 | 324 | -0.9 |
| 2C | 336 | 12.5 | 14.2 | 13.35 | 320 | 320 | 0 |
| 2C | 336 | 13.8 | 27.0 | 20.40 | 304 | 316 | -3.8 |
| 2C | 336 | 14.0 | 30.3 | 22.15 | 299 | 312 | -4.2 |
| 2C | 336 | 15.0 | 37.2 | 26.10 | 290 | 305 | -4.9 |
| 2C | 336 | 18.3 | 52.0 | 35.15 | 267 | 289 | -7.6 |
| 2C | 336 | 20.9 | 58.1 | 39.50 | 255 | 278 | -8.3 |
| 2C | 336 | 22.2 | 69.7 | 45.95 | 236 | 257 | -8.2 |
| 2D | 336 | 11.8 | 14.2 | 13.0 | 320 | 317 | +0.9 |
| 2D | 336 | 14.2 | 25.5 | 19.85 | 305 | 312 | -2.2 |
| 2D | 336 | 15.9 | 30.3 | 23.10 | 297 | 306 | -2.9 |
| 2D | 336 | 22.8 | 37.1 | 29.95 | 280 | 301 | -6.9 |
| 2D | 336 | 26.4 | 39.7 | 33.05 | 272 | 296 | -8.1 |
| 2D | 336 | 27.7 | 42.9 | 35.3 | 266 | 290 | -8.3 |
| 2D | 336 | 27.7 | 44.2 | 35.95 | 264 | 282 | -6.4 |
| 2D | 336 | 27.7 | 59.4 | 43.55 | 243 | 270 | -10.0 |
| 2D | 336 | 27.9 | 63.5 | 45.70 | 237 | 254 | -6.7 |

Figure 2.5 Predicted and Observed Resonant Frequencies at Various Crack Lengths in 85x180x3.2 mm Specimens Without Bonded Patches

Predicted and observed frequencies for 170x360 mm specimens having 1 and 3.2-mm thickness without bonded repairs are shown in Figures 2.6. The agreement between predictions and observed frequencies is within 10 percent except for specimen 3D in which the difference is over 10 percent for four crack lengths. For 3.2-mm thick specimens, the agreement between predictions and test results is within 10 percent even for large crack lengths (average crack length of 113.85 mm (4.5inch)).

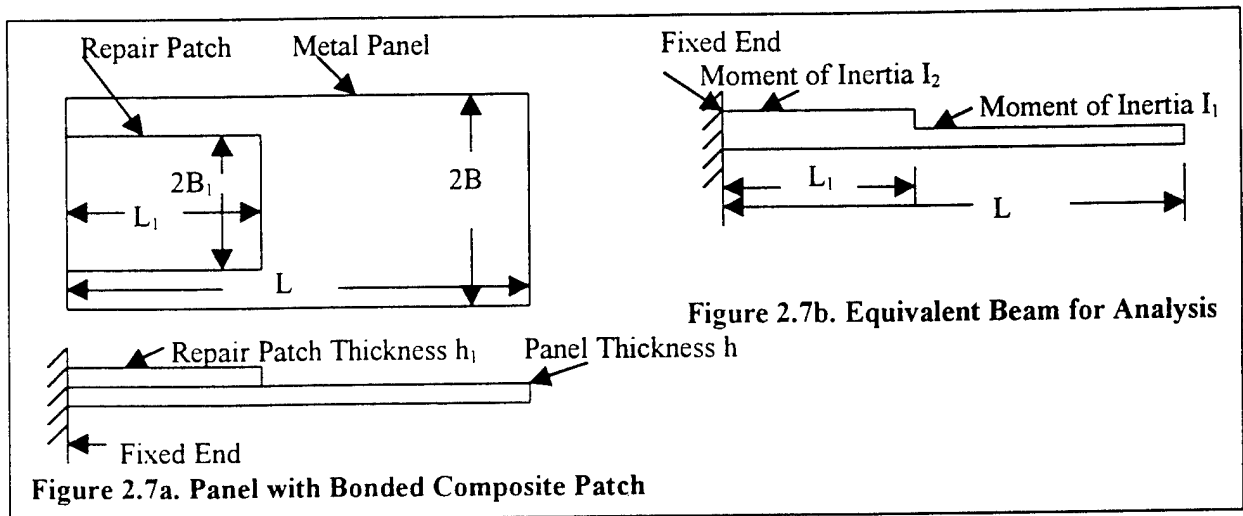
| Specimen ID | Test Frequency No Crack | Crack 1 (mm) | Crack 2 (mm) | Average Crack Length(mm) | Predicted Frequency | Test Frequency With Crack | Percentage Difference |
|--------------------------------|-------------------------|--------------|--------------|--------------------------|---------------------|---------------------------|-----------------------|
| TSP3 (1 mm thickness) | | | | | | | |
| 30 | 28 | 29.34 | 26.54 | 27.94 | 24.3 | 26 | -6.5 |
| 30 | 28 | 42.07 | 35.38 | 38.72 | 23.3 | 26 | -10.0 |
| 3A | 28 | 19.20 | 18.56 | 18.88 | 25 | 27 | -7.3 |
| 3A | 28 | 33.06 | 28.58 | 30.82 | 24 | 26 | -7.5 |
| 3B | 28 | 38.0 | 50.9 | 44.45 | 22.8 | 24 | -4.9 |
| 3B | 28 | 41.0 | 109.9 | 75.45 | 19.8 | 22 | -9.9 |
| 3C | 27 | 16.7 | 21.0 | 18.85 | 25.0 | 26 | -3.7 |
| 3C | 27 | 32.8 | 29.5 | 31.15 | 24.0 | 26 | -7.7 |
| 3D | 27 | 35.1 | 42.6 | 38.85 | 23.3 | 26 | -10.2 |
| 3D | 27 | 45.5 | 55.4 | 50.45 | 22.3 | 25 | -10.9 |
| 3D | 27 | 60.9 | 67.8 | 64.35 | 20.9 | 24 | -12.7 |
| 3D | 27 | 75.2 | 76.8 | 76.00 | 19.8 | 22 | -10.2 |
| 3D | 27 | 79.5 | 87.5 | 83.50 | 18.9 | 20 | -5.3 |
| 3D | 27 | 82.5 | 106.9 | 94.70 | 17.7 | 18 | -1.8 |
| TSP4 (3.2 mm thickness) | | | | | | | |
| 40 | 82 | 23.0 | 14.2 | 18.60 | 78.3 | 81 | -3.3 |
| 40 | 82 | 40.5 | 16.8 | 28.65 | 75.7 | 79 | -4.2 |
| 4A | 82 | 16.6 | 35.1 | 25.85 | 76.4 | 80 | -4.5 |
| 4A | 82 | 23.6 | 43.5 | 33.55 | 74.4 | 78 | -4.4 |
| 4A | 82 | 24.3 | 46.1 | 35.20 | 73.9 | 76 | -2.8 |
| 4B | 82 | 0.0 | 36.8 | 18.40 | 78.4 | 80 | -2.0 |
| 4B | 82 | 0.0 | 44.1 | 22.05 | 77.4 | 79 | -2.0 |
| 4C | 82 | 29.9 | 10.8 | 20.35 | 77.9 | 80 | -2.7 |
| 4C | 82 | 40.7 | 11.4 | 26.05 | 76.4 | 78 | -2.1 |
| 4C | 82 | 42.6 | 13.3 | 27.95 | 75.9 | 77 | -1.5 |
| 4C | 82 | 44.5 | 13.3 | 28.90 | 75.6 | 76 | -0.5 |
| 4D | 82 | 31.1 | 11.6 | 21.35 | 77.6 | 80 | -2.9 |
| 4D | 82 | 52.4 | 14.7 | 33.55 | 74.4 | 78 | -4.7 |
| 4D | 82 | 73.4 | 28.3 | 50.85 | 69.5 | 74 | -6.1 |
| 4D | 82 | 92.1 | 47.7 | 69.90 | 63.7 | 68 | -6.3 |
| 4D | 82 | 97.5 | 54.8 | 76.15 | 61.7 | 66 | -6.5 |
| 4D | 82 | 104.8 | 68.2 | 86.50 | 58.2 | 62 | -6.2 |
| 4D | 82 | 109.2 | 70.5 | 89.85 | 57.0 | 62 | -8.1 |
| 4D | 82 | 115.2 | 80.9 | 98.05 | 54.0 | 58 | -6.9 |
| 4D | 82 | 123.4 | 86.9 | 105.15 | 51.3 | 56 | -8.4 |
| 4D | 82 | 129.7 | 90.6 | 110.15 | 49.2 | 54 | -9.7 |
| 4D | 82 | 134.0 | 91.5 | 112.75 | 48.2 | 52 | -7.4 |
| 4D | 82 | 135.1 | 92.6 | 113.85 | 47.7 | 52 | -8.3 |

Figure 2.6 Predicted and Observed Resonant Frequencies at Various Crack Lengths in 170x360 mm Specimens (1 mm and 3.2 mm Thickness) Without Bonded Patches

Above results indicate that the simplified method proposed here gives good agreement with test results excepting for cases where crack lengths are large as compared to test specimen widths. This is perhaps due to the transverse local bending which results in significant displacement in transverse direction. Also, the assumption of effective panel width equal to actual panel width minus crack length may need modification for large crack lengths.

2.1.2 Resonant Frequencies of Panels With Bonded Patches

Analytical techniques were developed to predict resonant frequencies of panels with bonded patches. Rayleigh's method (Reference 11) was used to develop equations for resonant frequencies of bonded panels shown in Figure 2.7a. One-dimensional analysis was considered and the panel of Figure 2.7a was represented by a beam shown in Figure 2.7b. In the generalized formulation, developed here, the width and length of patch need not be the same as those of the panel.



The resonant frequency is given by (Reference 11)-

$$\omega_r = \left\{ \int_0^L E I(x) [\phi_r''(x)]^2 dx \right\} / \left\{ \int_0^L m(x) \phi_r^2(x) dx \right\} \quad (5)$$

where,

- ω_r = Resonant Frequency
- E = Young's Modulus
- I(x) = Moment of Inertia
- m(x) = Mass per unit length of the beam
- $\phi_r(x)$ = Function representing deflection curve of the beam
- $\phi_r''(x)$ = Second derivative of the deflection curve

The function $\phi_r(x)$ i.e. deflection curve is determined from the strength of materials type beam bending analysis. The deflection curve is give by-

$$d^2y/dx^2 = M(x)/[E I(x)] = \phi_r''(x) \quad (6)$$

where,

- $y(x) = \phi_r(x)$ = the deflection at distance x from the fixed end of the beam
- M(x) = Bending moment at distance x from fixed end of the beam
- I(x) = Moment of Inertia

In the present analysis, modulus E is assumed to be constant throughout the length of the beam. Although in most general case E can be function of distance x. The beam of Figure 2.7b is subjected to the loading due to the self weight of the panel and bonded patch as shown in Figure 2.8a. The deflection at any point C on the beam distance x from fixed end A is give by the moment of M/EI diagram between points A and C about C. The bending moment diagram for the beam is shown in Figure 2.8b and M/EI diagram is shown in Figure 2.8c.

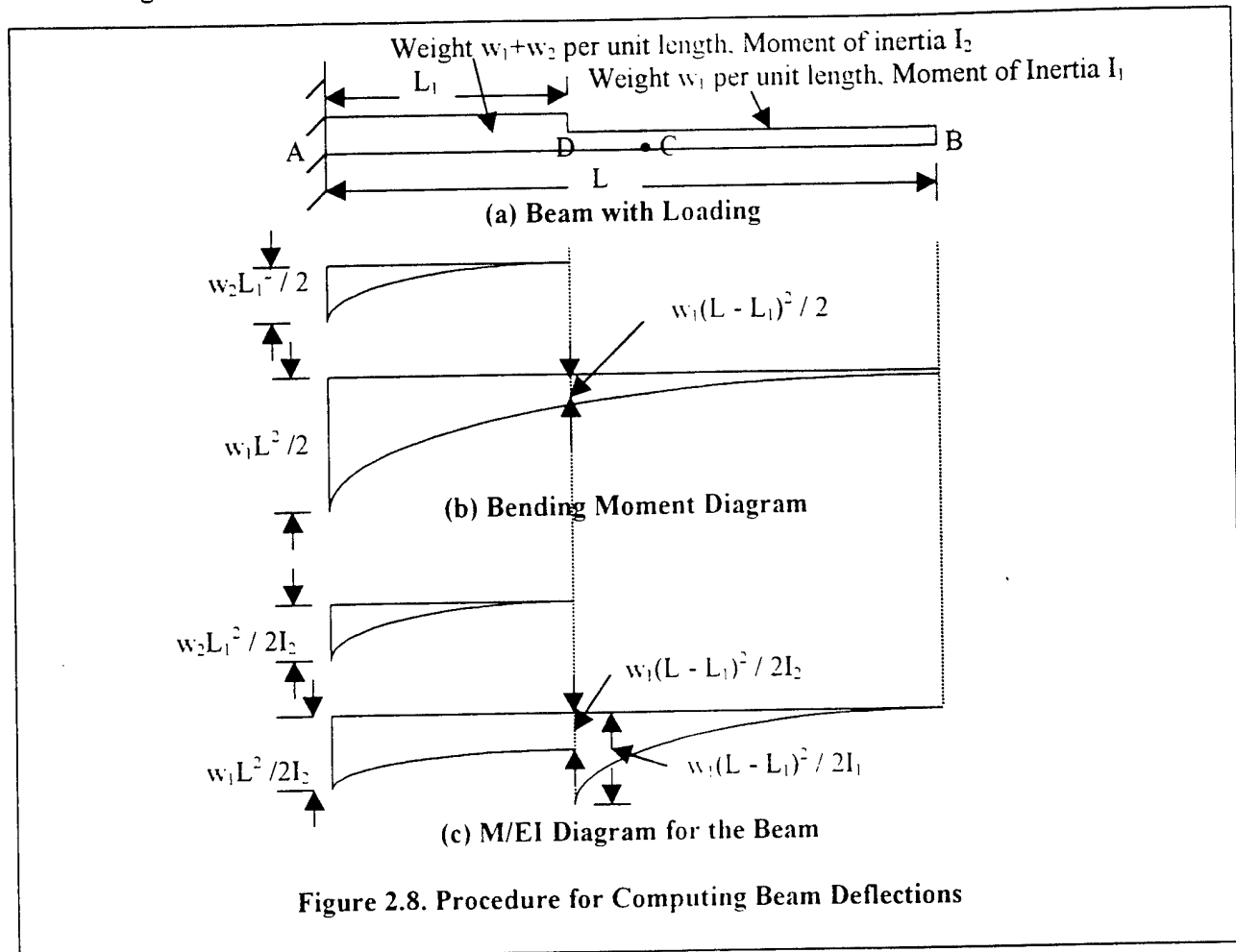


Figure 2.8. Procedure for Computing Beam Deflections

The deflection at a point C distance x from the fixed end is given by:

For $x < L_1$

$$y = \{w_2[(L_1-x)^4 + 4L_1^3 x - L_1^4] / 24EI_2\} + \{w_1[(L-x)^4 + 4L^3 x - L^4] / 24EI_2\} \quad (7)$$

For $x > L_1$

$$y = \{w_2 L_1^3 (4x - L_1) / 24EI_2\} + \{w_1[(L - L_1)^3 (3L_1 + L - 4x) + L^3 (4x - L)] / 24EI_2\} + \{w_1[(L - x)^4 + (L - L_1)^3 (4x - L - 3L_1)] / 24EI_1\} \quad (8)$$

The expressions for bending moment M(x) are given by-

For $x < L_1$

$$M(x) = -w_1(L-x)^2 / 2 - w_2(L_1-x)^2 / 2 \quad (9)$$

For $x > L_1$

$$M(x) = -w_1(L-x)^2/2 \tag{10}$$

Substituting Equations 7-10 in Equation 5 and integrating, expression for resonant frequency is obtained. The integration becomes rather cumbersome and to simplify the algebra involved, the effect of weight w_2 of the patch on bending moment is neglected. As the total weight of patch is small as compared to the total weight of the panel and the fact that the weight is located near the support it's effect on bending moment, hence, resonant frequency will be small. This assumption simplifies algebra significantly. A FORTRAN computer program is written to obtain resonant frequencies. The computer program has following inputs-

- 1) Panel- width, length, thickness, modulus, density.
- 2) Repair Patch- width, length, thickness, modulus, density.

It may be noted that the panels bonded with composite patches have cracks present and to account for the presence of cracks in panels, moment of inertia of uncracked panel section is used in computations. The computer program was used to obtain resonant frequencies for various patched panels tested in References 3-4. A patch thickness of 0.09-inch and patch modulus of 7×10^6 psi were used in computing the resonant frequencies. A comparison of predicted and observed resonant frequencies is shown in Figure 2.9. As shown in the figure, agreement between test results and analytical predictions is good except for one thick small panel. It may be noted that each panel has two cracks and average crack length is used to predict resonant frequencies.

| Specimen Series | Width (mm) | Length (mm) | Thickness (mm) | Crack Lengths (mm) | Predicted Frequency(Hz) | Test Frequency(Hz) | Percentage Difference (Average Based) |
|-----------------|------------|-------------|----------------|--------------------|-------------------------|--------------------|---------------------------------------|
| 1 | 85 | 180 | 1 | 24.9, 25.8 | 155.5 | 166 | +6.7 |
| 1 | 85 | 180 | 1 | 27.3, 21.4 | 156.7 | 158 | +0.8 |
| 1 | 85 | 180 | 1 | 27.3, 23.6 | 155.3 | 158 | +1.7 |
| 2 | 85 | 180 | 3.2 | 26.1, 10.4 | 443.0 | 385 | -13.0 |
| 2 | 85 | 180 | 3.2 | 26.8, 12.3 | 439.8 | 396 | -9.9 |
| 2 | 85 | 180 | 3.2 | 46.1, 13.0 | 410.3 | 402 | -2.0 |
| 3 | 170 | 360 | 1 | 42.07, 35.38 | 29.4 | 32 | +8.8 |
| 3 | 170 | 360 | 1 | 28.58, 33.06 | 30.3 | 32 | +5.6 |
| 3 | 170 | 360 | 1 | 32.8, 29.5 | 30.2 | 31 | +2.6 |
| 4 | 170 | 360 | 3.2 | 40.5, 16.8 | 87.9 | 86 | -2.2 |
| 4 | 170 | 360 | 3.2 | 24.3, 46.1 | 86.1 | 88 | +2.3 |
| 4 | 170 | 360 | 3.2 | 0, 44.1 | 89.7 | 87 | -3.0 |

Figure 2.9 Predicted and Observed Resonance Frequencies In Panels With Bonded Composite Patches

2.2 Dynamic Stress Analysis of Vibrating Panels and Verification With Test Data

Dynamic stress analysis was developed for the panels tested by WPAFB under vibratory loads with base excitation. The analysis was used to predict strains in the panels and compare with test results.

2.2.1 Dynamic Stress Analysis

The panel geometry shown in Figure 2.1a was considered. Due to symmetry of the panel and deflection curve, only one half of the panel is considered. Thus, the solution to problem reduces to that of vibrating panel shown in Figure 2.10. The base is excited and vibrates with displacement given by: $z = z_0 e^{i\Omega t}$

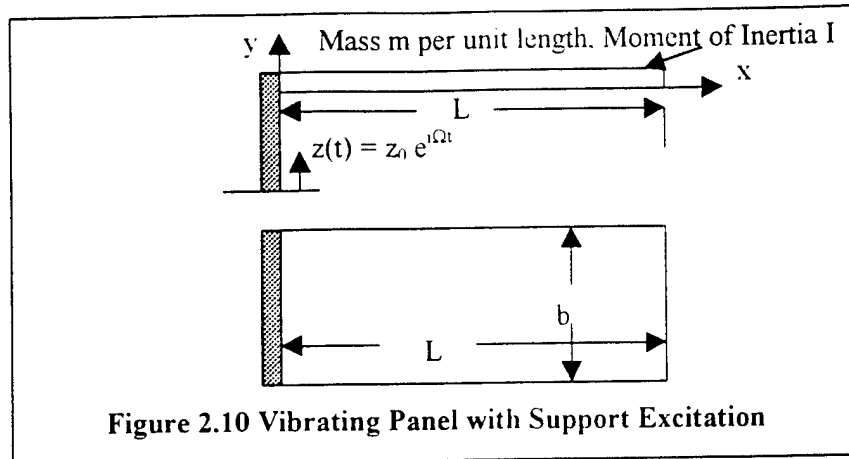


Figure 2.10 Vibrating Panel with Support Excitation

The differential Equation of the vibrating panel is given by:

$$D \frac{\partial^4 w}{\partial x^4} = q = -(\gamma b h / g) \frac{\partial^2 z}{\partial t^2} \quad (11)$$

Where,

w = Deflection of the panel in z direction

h = Panel thickness

b = Panel width

γ = Weight density of panel material

g = Acceleration due to gravity

D = Flexural Rigidity of the Panel = $bh^3/[12(1-\nu^2)]$

The deflection of the panel as a function of time may be written as

$$w(x,t) = \varphi(\beta x) \eta(t) \quad (12)$$

For a clamped panel with vibrating fixed end, the displacement w is given by:

$$w = z(t) + \varphi(\beta x) \eta(t) \quad (13)$$

Substituting Equation (13) in Equation (11), gives

$$D\beta^4 \varphi(\beta x) \eta(t) = -(\gamma b h / g) z(t) - (\gamma b h / g) \eta(t) \quad (14)$$

Multiplying both sides by $\varphi(\beta x)$ and integrating from 0 to L.

$$\int_0^L D\beta^4 \varphi^2(\beta x) \eta(t) + (\gamma b h / g) \int_0^L \varphi^2(\beta x) \eta(t) = -(\gamma b h / g) \int_0^L \varphi(\beta x) z(t) \quad (15)$$

Note the following integrals for the case of a cantilever of span L (Reference 12)

$$\int_0^L \varphi^2(\beta x) dx = L, \quad \int_0^L \varphi(\beta x) dx = 2\alpha / \beta. \quad (16)$$

For fundamental mode 1, $\alpha = 0.734$, $\beta = 1.875$

Note that

$$z = z_0 e^{i\Omega t}, \quad \ddot{z} = -z_0 \Omega^2 e^{i\Omega t}$$

Using integrals given by Equation (16) in Equation (15).

$$D\beta^4 L \eta(t) + (\gamma b h / g) L \ddot{\eta}(t) = (\gamma b h / g) (2\alpha / \beta) z_0 \Omega^2 e^{i\Omega t} \quad (17)$$

Define, $D\beta^4 L = K$

$$(\gamma b h / g) L = M$$

Equation (17) reduces to:

$$K \eta(t) + M \ddot{\eta}(t) = (\gamma b h / g) (2\alpha / \beta) z_0 \Omega^2 e^{i\Omega t} \quad (18)$$

$$\ddot{\eta}(t) + (K/M) \eta(t) = [\gamma b h / (gM)] (2\alpha / \beta) z_0 \Omega^2 e^{i\Omega t} \quad (19)$$

Define $K/M = \omega^2$, Equation (19) reduces to:

$$\ddot{\eta}(t) + \omega^2 \eta(t) = [\gamma bh/(gM)] (2\alpha/\beta) z_0 \Omega^2 e^{i\Omega t} \quad (20)$$

If damping of the panel is considered, Equation (20) becomes

$$\ddot{\eta}(t) + 2\zeta\omega\dot{\eta}(t) + \omega^2 \eta(t) = [\gamma bh/(gM)] (2\alpha/\beta) z_0 \Omega^2 e^{i\Omega t} \quad (21)$$

Where,

$$\zeta = \text{Damping ratio} = c / [2 (KM)^{1/2}]$$

c = Viscous damping coefficient

The solution to Equation (21) is given by:

$$\eta(t) = \{[\gamma bh/(gM)] (2\alpha/\beta) z_0 \Omega^2 e^{i\Omega t}\} / \{[(\omega^2 - \Omega^2)^2 + 4 \zeta^2 \Omega^2]^{1/2}\} \quad (22)$$

$$\eta(t) = \{[\gamma bh/(gK)] (K/M)(2\alpha/\beta) z_0 \Omega^2 e^{i\Omega t}\} / \{[(\omega^2 - \Omega^2)^2 + 4 \zeta^2 \Omega^2]^{1/2}\} \quad (23)$$

$$\eta(t) = \{[\gamma bh/(gK)] (2\alpha/\beta) z_0 \Omega^2 e^{i\Omega t}\} / \{[1 - (\Omega/\omega)^2]^2 + 4 \zeta^2 (\Omega/\omega)^2\}^{1/2} \quad (24)$$

The displacement w of the panel is given by Equation (12). Maximum deflection occurs at free end at x = L. For a cantilever panel at x = L, $\phi(\beta L) = 2$, and deflection is given by:

$$w(L,t) = 2 \eta(t) \quad (25)$$

Strain in the panel is given by $e_x = z (d^2w/dx^2)$ and maximum strain occurs at $z = \pm h/2$.

Under harmonic excitation at fundamental vibrating frequency $\omega = \Omega$, the maximum strain is:

$$e_x = (h/4\zeta)[\gamma bh/(gK)] (2\alpha/\beta) z_0 \Omega^2 e^{i\Omega t} (d^2\phi/dx^2) \quad (26)$$

At x = 0 (fixed end of the panel), $(d^2\phi/dx^2) = 2\beta^2$ (Reference 12)

Equation (26) reduces to:

$$e_x = [\gamma bh^2\alpha/(gD\beta^3L\zeta)] z_0 \Omega^2 e^{i\Omega t} \quad (27)$$

Note- $z_0 \Omega^2 e^{i\Omega t} = z(t) = \text{Input acceleration to the vibrating panel}$

2.2.2 Comparison Between Predictions and Test Data

Test data provided by WPAFB (References 1-4) was used to verify dynamic analysis discussed above. In the tests conducted at WPAFB, test panels with various dimensions were vibrated by a shaker. Tip displacements were measured for various specimens. Using these tip displacements, and simple beam theory maximum strains were obtained for various test specimens. These tip displacements were provided by Mr. David Banaszak of WPAFB and are shown in Figure 2.11 along with dimensions of the test specimens. The figure also shows the input g loading for each specimen.

| Test Series | Number of Specimens | Specimen Size inch (mm) | Specimen Thickness inch (mm) | Input g Loading | Tip Displacement inch(mm) |
|-------------|---------------------|-------------------------|------------------------------|-----------------|---------------------------|
| 1 | 3 | 7.1x3.3(180x85) | 0.04(1mm) | 6 | 0.5(12.7) |
| 2 | 3 | 7.1x3.3(180x85) | 0.125(3mm) | 6 | 0.175(4.45) |
| 3 | 3 | 14.2x6.7(360x170) | 0.04(1mm) | 3 | 2.00(50.8) |
| 4 | 3 | 14.2x6.7(360x170) | 0.125(3mm) | 3 | 0.675(17.15) |

Figure 2.11 Details of Specimen Configurations Tested by WPAFB

The displacement for each of specimen series were used in Equation (25) to compute damping ratio ζ and viscous damping coefficient c for each of the specimen series. These values are shown in Figure 2.12.

These values of damping coefficient factor were used in strain Equation (27) to obtain maximum strains in the beam. The values of $z_0 \Omega^2 e^{i\Omega t} = z(t)$ are the input g values given in Figure 2.11. The predicted strain values are shown in Figure 2.12. The figure also shows the strain values obtained by the Air Force using simple beam theory and experimentally obtained deflections. Predicted strains obtained by dynamic analysis agree well with those obtained by the Air Force from tip deflections.

| Specimen Size (in) | Resonance Frequency | Input g Loading | Damping Ratio(ζ) | Damping Coefficient (c) | Strains(μ in/in) Predicted | Strains(μ in/in) Test | Difference % |
|--------------------|---------------------|-------------------|--------------------------|-------------------------|---------------------------------|----------------------------|--------------|
| 7.1x3.3x0.04 | 112 | 6 | 0.0093 | 0.00024 | 3.088 | 3.187 | +3.1 |
| 7.1x3.3x0.125 | 348 | 6 | 0.0028 | 0.000707 | 3.377 | 3.346 | -0.9 |
| 14.2x6.7x0.04 | 27 | 3 | 0.0205 | 0.00026 | 2.941 | 3.187 | +7.7 |
| 14.2x6.7x0.125 | 83 | 3 | 0.0056 | 0.000707 | 3.101 | 3.226 | +3.8 |

Figure 2.12 Comparison of Predicted and Test Strains

2.2.3 Comparison Between Dynamic and Static Deflection Curves

Static analysis of the vibrating panel shown in Figure 2.11 was carried out and deflection curve obtained assuming uniform load on the panel. A comparison of deflections obtained from dynamic analysis (Equation 12) and static analysis, using uniform loading corresponding to maximum experimental tip deflections, is shown in Figure 2.13. The figure shows a very good agreement. This good correlation between deflection curves is the reason for good correlation between strains shown in Figure 2.12.

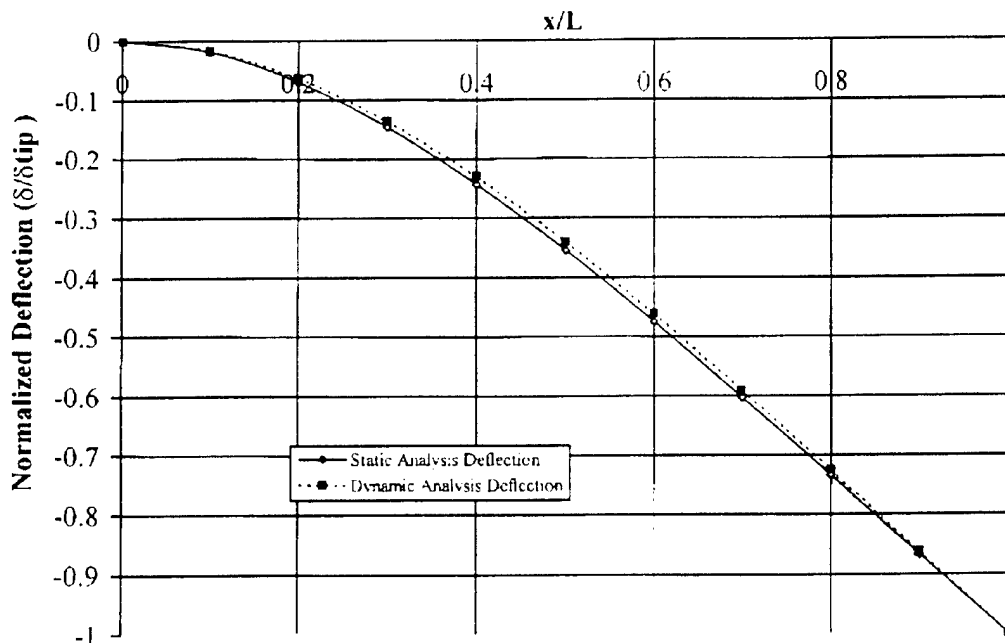


Figure 2.13 Comparison of Static and Dynamic Deflection Curves

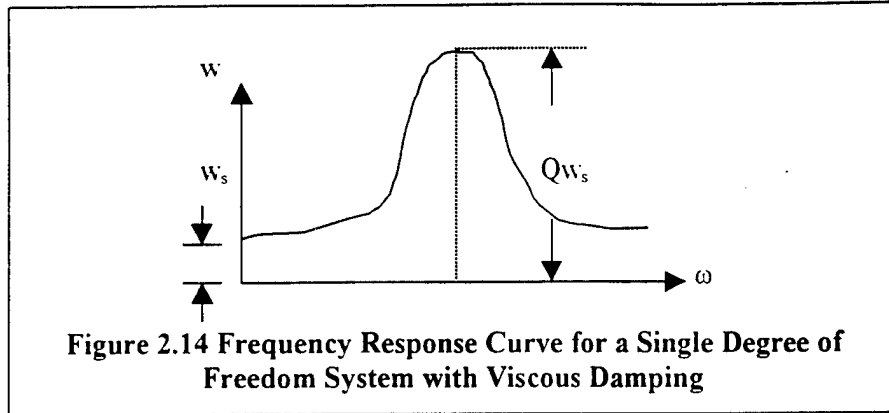
2.3 Damping Ratio ζ Computations from Magnification Factor

Reference 13 has shown that the relationship between damping ratio ζ and dynamic magnification factor Q as:

$$Q = 1/2\zeta \quad (28)$$

Or $\zeta = 1/2Q \quad (29)$

A typical frequency response curve for a single degree of freedom system with viscous damping is shown in Figure 2.14. The displacement increases sharply and reaches maximum value when resonance occurs. The maximum displacement is Q times static displacement w_s , where Q is known as the dynamic magnification factor. The value of Q is given by Equation 28.



Test data provided by WPAFB on specimen configuration of Figure 2.1 was used to verify the validity of Equation 29. The maximum tip deflections at resonance frequencies were measured in the specimens and are shown in Figure 2.11. The maximum tip deflection for a cantilever with uniform load is given by:

$$w_s = w L^4 / (8EI) \quad (30)$$

where,

w_s = maximum tip deflection

w = Uniformly distribute load per unit length of the beam

L = Span of the beam

E = Young's Modulus

I = Moment of inertia

For the panels tested in References 1-4.

$$I = bh^3 / [12(1-\nu^2)]$$

$$w = \rho bh(g/g)$$

where,

ρ = Mass density of the beam material

g = Acceleration due to gravity

g_i = Maximum input excitation acceleration in the vibrating panel

Equation (30) was used to compute static deflection for each of the four panel configurations shown in Figure 2.11. Using the computed static deflections and the dynamic test deflections data provided by the Air Force, the values of magnification factor Q were computed. These values of Q were used in Equation 29 to compute damping ratios ζ and are shown in Figure 2.15. The figure also shows the values of damping ratio ζ computed from dynamic analysis discussed earlier (Figure 2.12). The agreement between the values, obtained by two methods, is very good.

| Test Series | Specimen Size (in) | Resonance Frequency | Input rms g | Static Tip Deflection | Dynamic Tip Deflection | Q | Damping Ratio(ζ) | Damping Ratio ζ (Figure 2.12) |
|-------------|--------------------|---------------------|-------------|-----------------------|------------------------|--------|--------------------------|-------------------------------------|
| 1 | 7.1x3.3x0.04 | 112 | 6 | 0.0094 | 0.5 | 53.19 | 0.0094 | 0.0093 |
| 2 | 7.1x3.3x0.125 | 348 | 6 | 0.00096 | 0.175 | 182.29 | 0.0027 | 0.0028 |
| 3 | 14.2x6.7x0.04 | 27 | 3 | 0.0826 | 2.0 | 24.21 | 0.0206 | 0.0205 |
| 4 | 14.2x6.7x0.125 | 83 | 3 | 0.00829 | 0.675 | 81.42 | 0.0061 | 0.0056 |

Figure 2.15 Comparison of Damping Ratios

SECTION 3

CRACK GROWTH UNDER VIBRATORY LOADS

3.1 Review of Fatigue Crack Growth Test Data

Raw data generated by Mr. David Banaszak at Wright Patterson Air Force Base (References 1-4) was provided to R-Tec by the Air Force. Fatigue crack growth test data on specimens with and without bonded patches, provided to R-Tec, were reviewed to get a better understanding of the influence of various parameters such as panel length and thickness on crack growth. The test data provided by the Air force are on four series of specimens with dimensions and load levels shown in Figure 2.11. All the testing was done with sinusoidal excitation under constant amplitude loading. These data are discussed in the following subsections.

3.1.1 Fatigue Crack Growth Behavior Including Crack Initiation

The fatigue crack growth of Test Series 1 specimens is shown in Figure 3.1. The number of fatigue cycles shown in the figure includes initiation cycles. The test data shows a large scatter in number of cycles to first crack detection. The numbers of cycles vary from 40,000 to 120,000 at the first observed crack length of about 0.4-inch (10-mm). This scatter in data is not unusual when crack initiation is included in crack growth life.

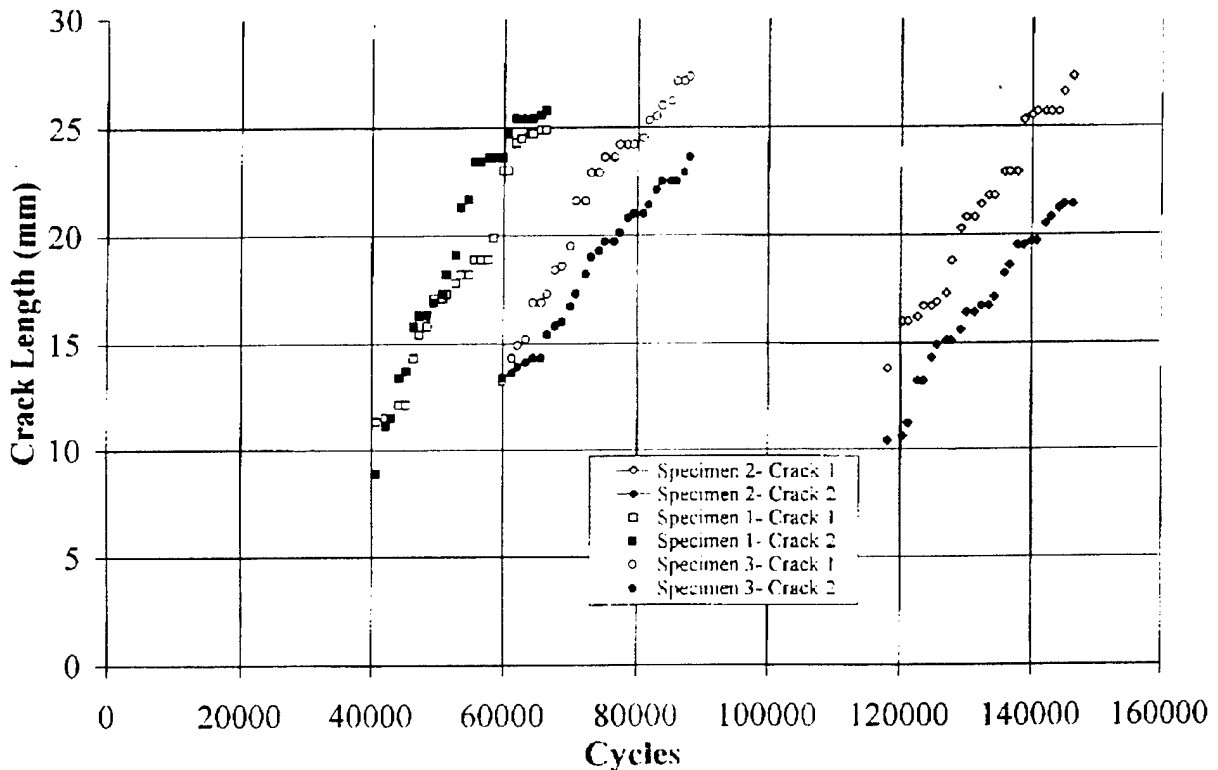


Figure 3.1 Crack Growth in Test 1 Specimens (Initiation Included)

The fatigue behavior of Test Series 2 specimens is shown in Figure 3.2. The test data from this series of specimens show less scatter. Numbers of cycles to first crack detection are not much different for 3 specimens. An interesting thing to note is that growth of one crack in each specimen increases with number of cycles, however, the second crack in each specimen is retarded and shows very little growth.

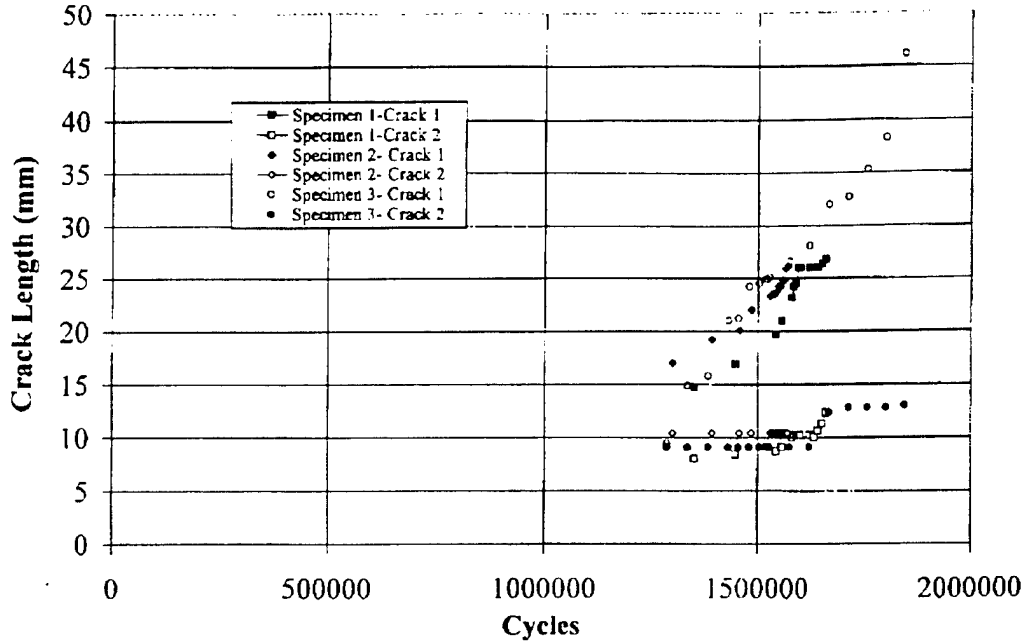


Figure 3.2 Crack Growth in Test Series 2 Specimens (Initiation Included)

The fatigue behavior of Series 3 specimens is shown in Figure 3.3. The test data show much less scatter. Number of cycles to first crack detection is not much different for 3 specimens. An interesting thing to note is that the fatigue cycles to 0.4-inch (10-mm) crack in Series 1 specimen are much more as compared to those for Series 3 specimens, even though both the specimen series have same thickness and same maximum strain at the root (crack initiation site) as indicated in Figure 2.12. The maximum strain in both the specimens, corresponding to maximum tip deflection for each specimen, is 3,187 micro inch/inch. The difference in crack growth life is attributed to dynamic effects. The test resonant frequencies for series 1 specimens are between 110 to 112 Hz and for Series 3 specimens between 27 to 28. Thus, the resonant frequencies for Series 1 specimens are 4 four times those for Series 3 specimens. These results indicate that effect of dynamic loading frequencies has to be considered in any prediction methodology.

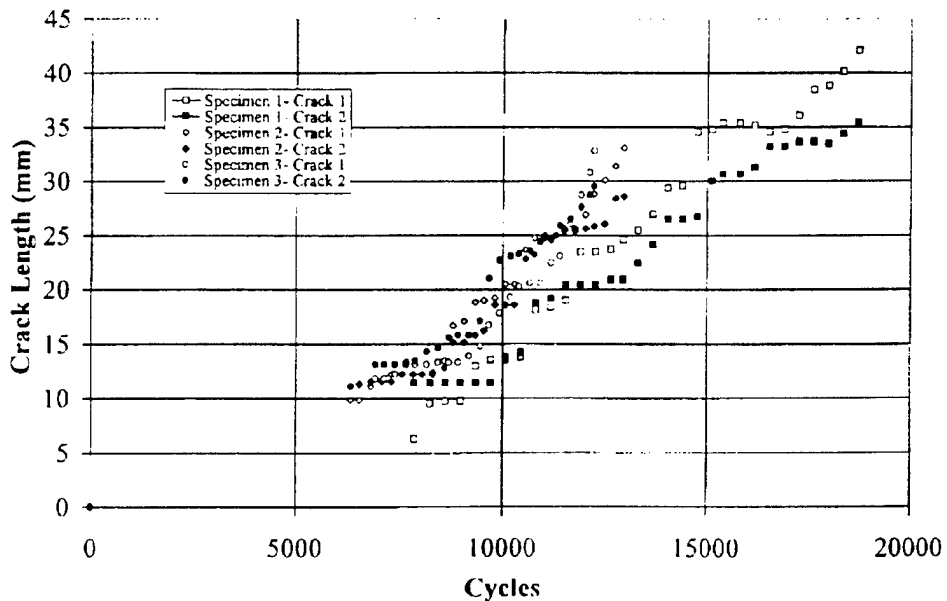


Figure 3.3 Crack Growth in Test Series 3 Specimens (Initiation Included)

The fatigue behavior of Series 4 specimens is shown in Figure 3.4. The test data show a large scatter. A comparison of Series 2 (Figure 3.2) and Series 4 (Figure 3.4) test data shows that cycles to 0.4-inch (10-mm) crack for Series 4 specimens are less as compared to those for Series 2 specimens, even though both the specimen series have same thickness and about the same maximum strain at the root (crack initiation site) as shown in Figure 2.12. The maximum strain in Series 2 specimens is 3.346 micro inch/inch and in Series 4 specimens 3.226 micro inch/inch. The test resonant frequencies for Series 2 specimens are between 330 to 336 Hz and for Series 4 specimens between 82 to 83.

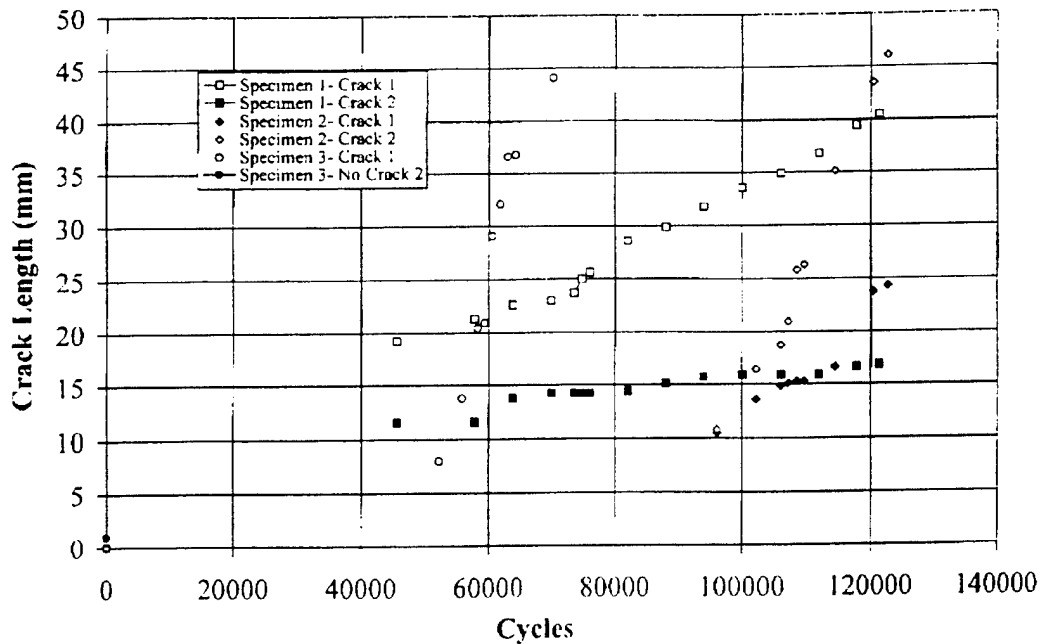


Figure 3.4 Crack Growth in Test Series 4 Specimens (Initiation Included)

3.1.2 Fatigue Crack Growth Behavior After First Crack Detection

In view of significant scatter in observed fatigue test data that included crack initiation, the test data provided by WPAFB were analyzed to investigate only crack growth behavior under vibratory loading. For each specimen of data series shown in Figure 3.1, the crack growth was plotted as a function of number of cycles after the first crack was detected in each specimen. Thus, for each specimen the time at which first crack was observed was considered as starting point with zero cycles and cycles were counted from this point onwards for comparing crack growth behavior.

The crack growth behavior of Series 1 specimens after first crack was detected is shown in Figure 3.5. As seen in the figure, the crack growth data show less scatter as compared to when initiation life was included (Figure 3.1). The crack growth rate increases uniformly as crack length increases, however, after about 15,000 cycles, rate of increase in crack growth rate slows down. The slowing down in crack growth rate is attributed to interaction between parallel cracks. As shown in Figure 2.3 two cracks initiate in each specimen, on either side of specimen centerline. The parallel cracks shield each other and reduce stress intensity factors, hence, crack growth rate.

The crack growth data for Test Series 2-4 specimens are shown in Figures 3.6-3.8. The crack growth data for specimen Series 2 in Figure 3.6 show a large difference in crack growth rates for crack 1 and crack 2 in each specimen. One crack in each of Series 2 specimens is retarded and grows at very slow rate.

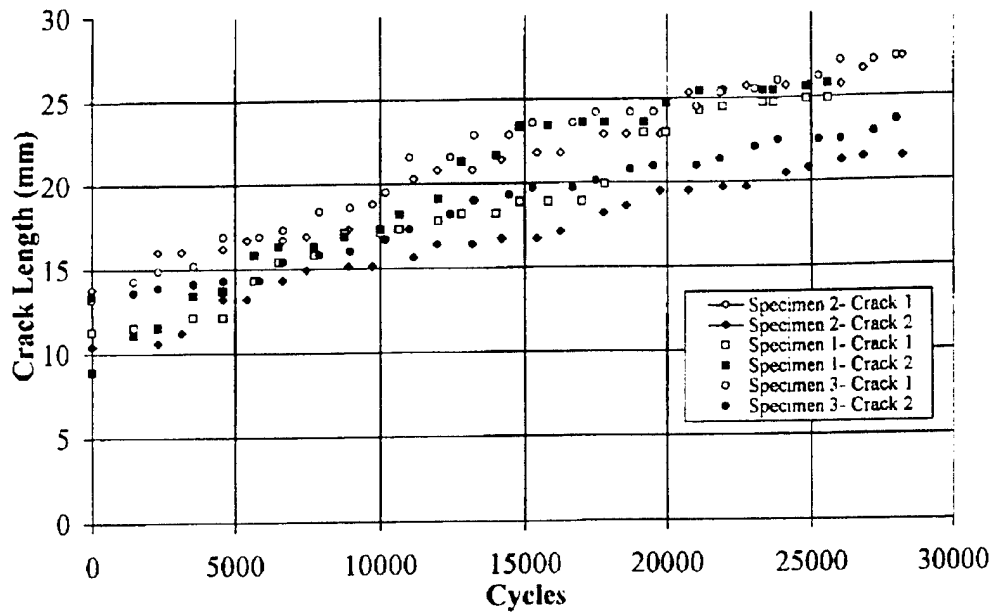


Figure 3.5 Crack Growth in Test Series 1 Specimens (After First Crack Detection)

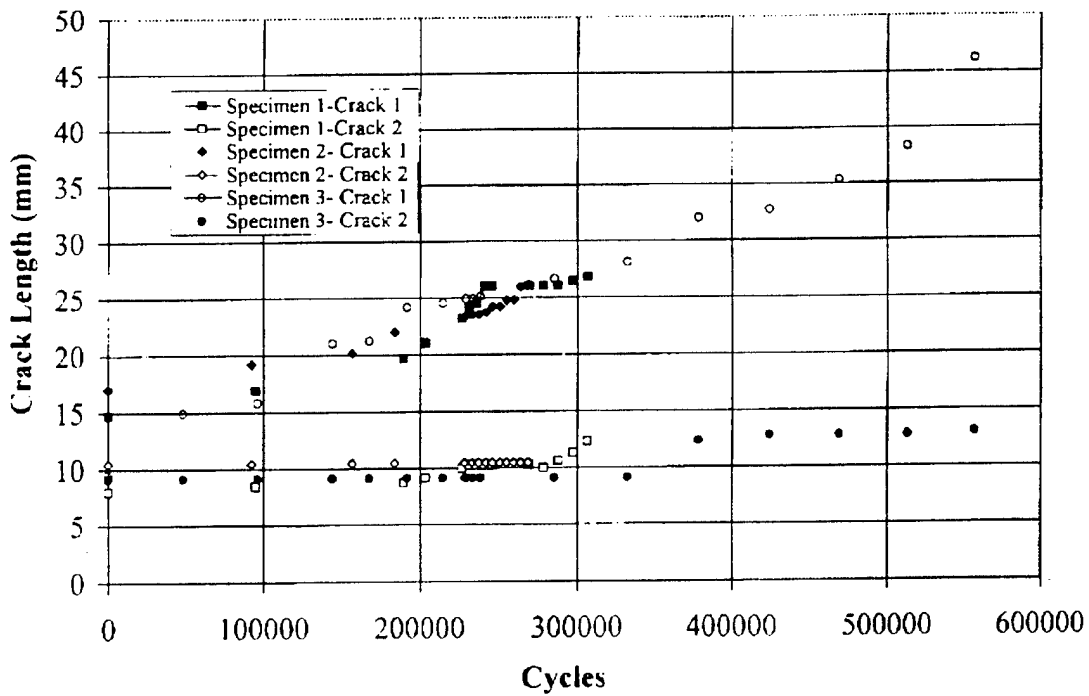


Figure 3.6 Crack Growth in Test Series 2 Specimens (After First Crack Detection)

Test Series 3 specimens in Figure 3.7 show less scatter in crack growth data. The crack growth rate increases uniformly up to about 6,000 cycles and then slows down as for test Series 1 specimens. The crack growth data for Series 4 specimens in Figure 3.8 show large scatter. Figures 3.5-3.8 test data show that 0.04-inch (1-mm) thick specimens show less scatter in crack growth data compared to 0.125-inch (3.2-mm) thick specimens.

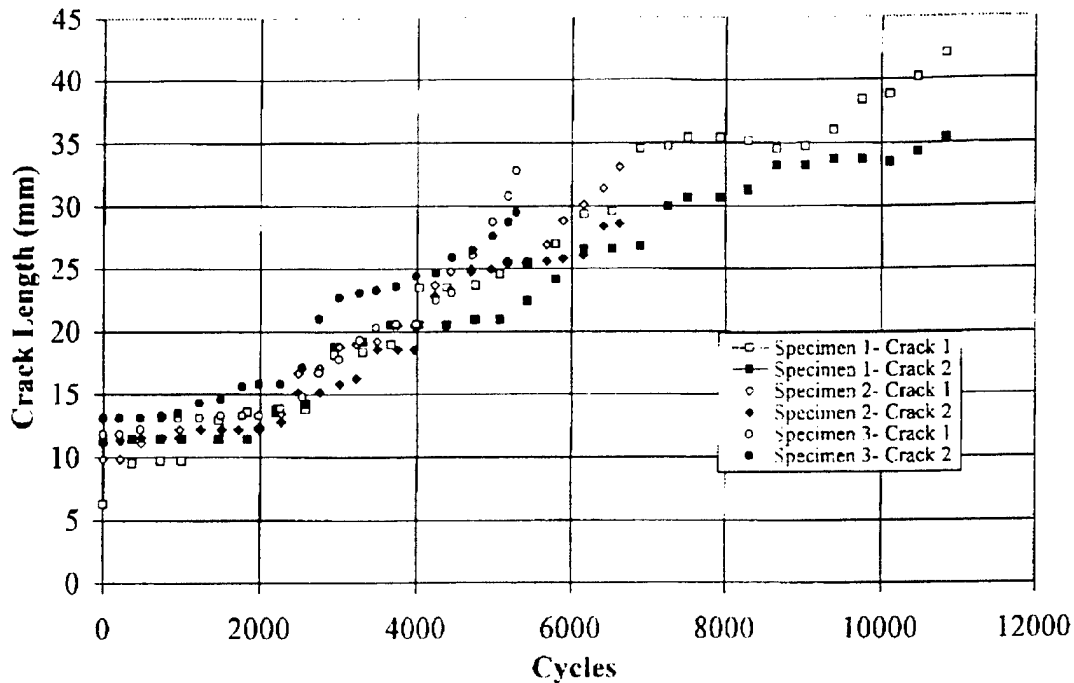


Figure 3.7 Crack Growth in Test Series 3 Specimens (After First Crack Detection)

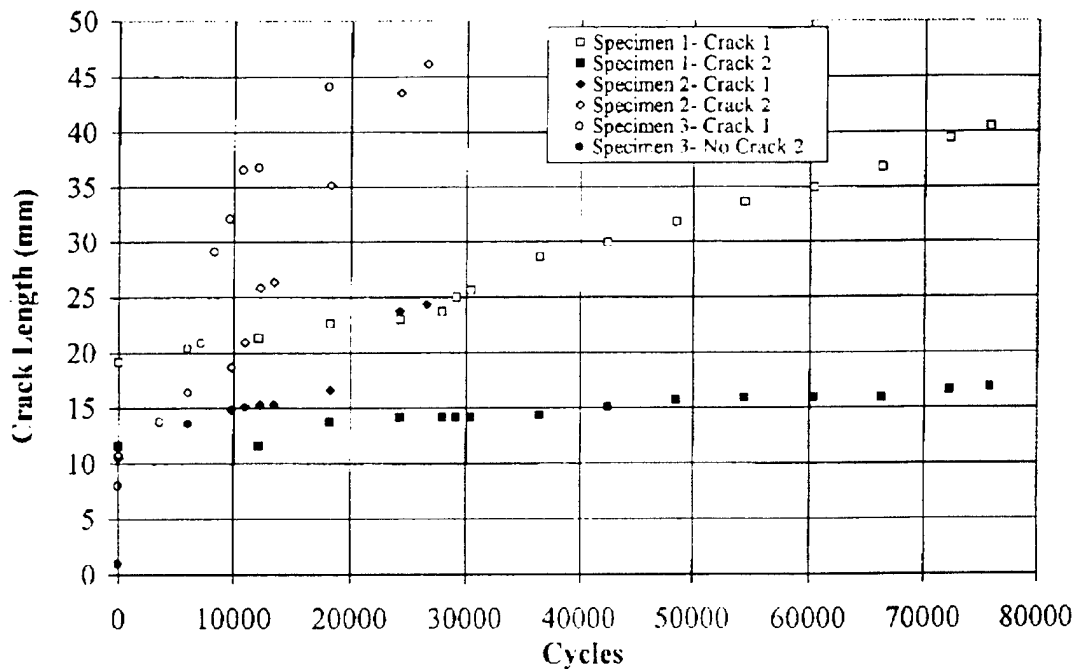


Figure 3.8 Crack Growth in Test Series 4 Specimens (After First Crack Detection)

The WPAFB test specimens were examined to understand the reason for large scatter in thick test specimens. It was found that in the thick specimen cracks on two surfaces of the specimens did not initiate in the same through-the-thickness plane under vibratory loads. The test specimens were subjected to fully reversed bending loads ($R = -1$, where R is ratio of minimum to maximum stress in fatigue). In the thick specimens, cracks initiate as surface cracks in different planes on two surfaces. Some thick test specimens showed three cracks, two on one side of specimen centerline and one on the other side.

3.1.3 Comparison of Fatigue Crack Growth Behavior in Test Specimens

A comparison of crack growth behavior in Test Series 1 and 2 is shown in Figure 3.9. The specimens in the tests are made from same material and have the same size (Length and Width). However, the thickness of Test Series 2 specimens is three times that of Test Series 1. The maximum strains in both the specimen series are almost the same. Hence, crack growth behavior is expected to be similar. However, Figure 3.9 indicates the crack growth in Test Series 1 to be faster compared to Test Series 2. The resonant frequency of Test Series 2 specimens (330-336 Hz) is 3 times that for Test Series 1 specimens (110-112 Hz). It is shown in Reference 14 that higher frequency causes reduction in stress intensity factors, hence, slower crack growth. Also, cracks do not initiate in the same plane in thicker specimens under fully reversed bending. Hence, instead of one crack on each side of specimen centerline there may be two parallel cracks that try to shield each other. This will reduce stress intensity factors and crack growth rate.

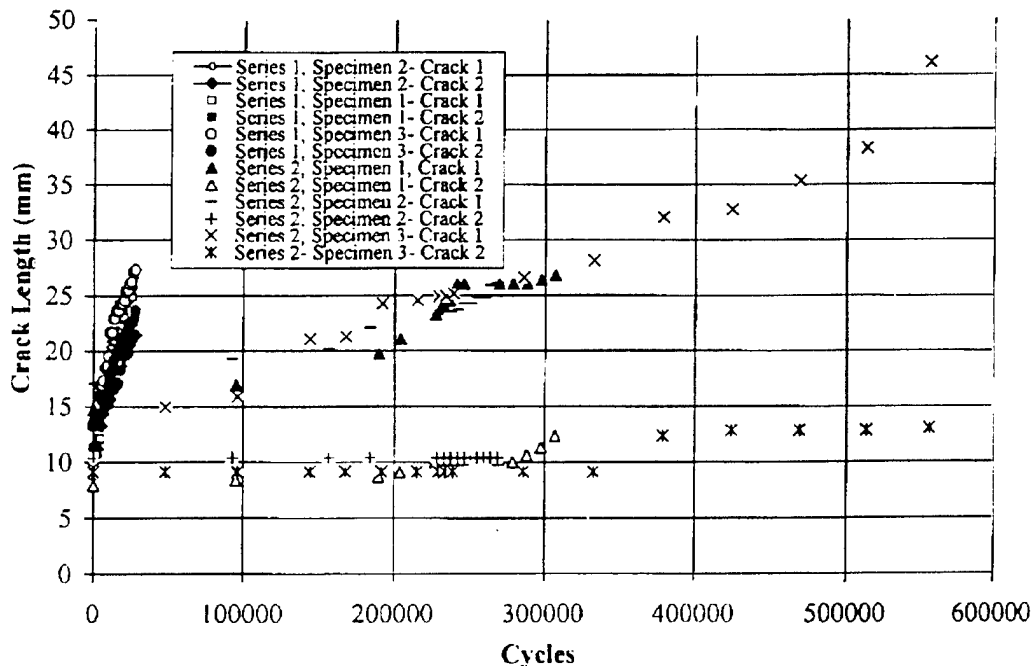


Figure 3.9 Comparison of Crack Growth in Test Series 1 and 2 Specimens (After First Crack Detection)

A comparison of crack growth in Test Series 1 and 3 is shown in Figure 3.10. Test specimen Series 1 and 3 are of same material and thickness with almost same maximum strains as indicated in Figure 2.12. However, size of specimens (length and width) in Test Series 3 is twice that in Test Series 1. In view of similar strains in two specimen series, crack growth behavior is expected to be same. However, Figure 3.10 indicates the crack growth in Test Series 3 to be much faster as compared to Test Series 1. This is attributed to different test frequencies (resonant frequencies) of the test series. The resonant frequency of specimens in Test Series 1 (110-112Hz) is 4 times that for Test Series 3 (27-28 Hz).

A comparison of crack growth behavior in Test Series 2 and 4 is shown in Figure 3.11. The specimens in these test series are made from same material and have same thickness. However, size of specimens (Length and Width) in Test Series 4 is twice that of Test Series 2. The maximum strain in both the specimen series is almost the same. Hence, crack growth behavior is expected to be similar. However, Figure 3.10 indicates the crack growth in Test Series 4 to be much faster as compared to Test Series 2. The test frequencies (resonant frequencies) of two specimen series are different. The resonant frequency of Test Series 2 specimens (330-336 Hz) is 4 times that for Test Series 4 specimens (82-83 Hz). It is shown in Reference 14 that higher frequency causes reduction in SIFs, hence, slower crack growth.

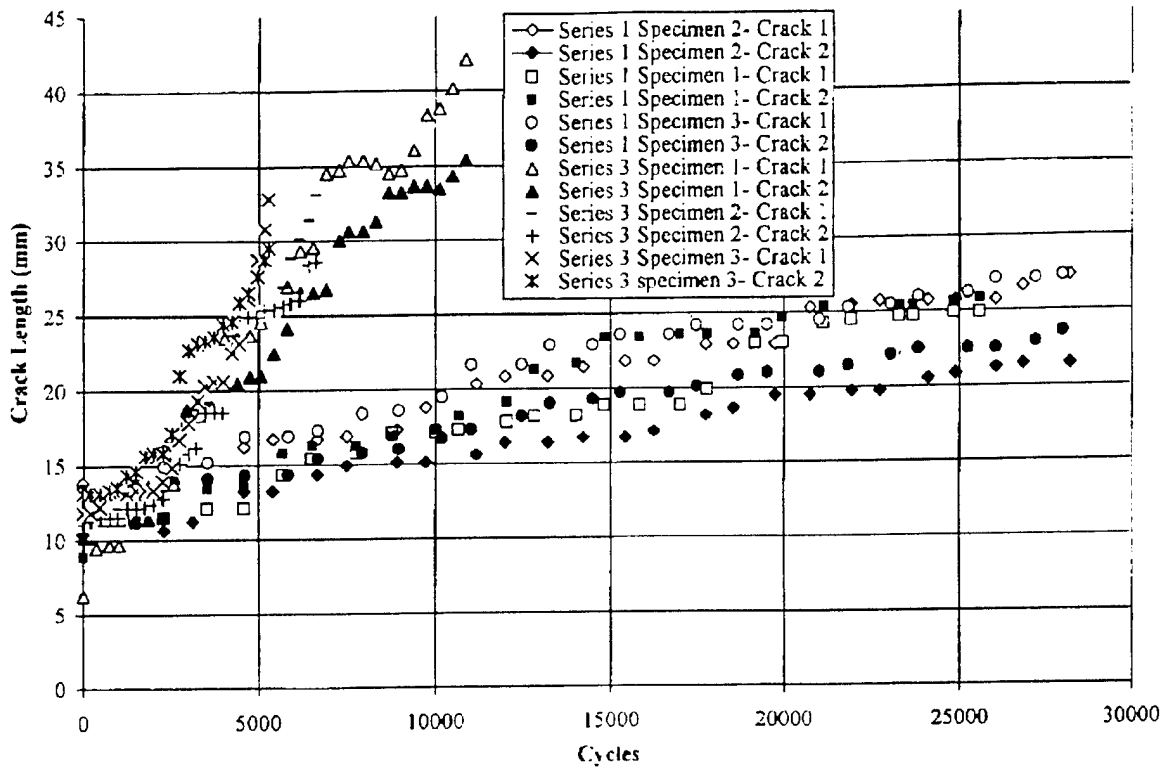


Figure 3.10 Comparison of Crack Growth in Test Series 1 and 3 Specimens (After First Crack Detection)

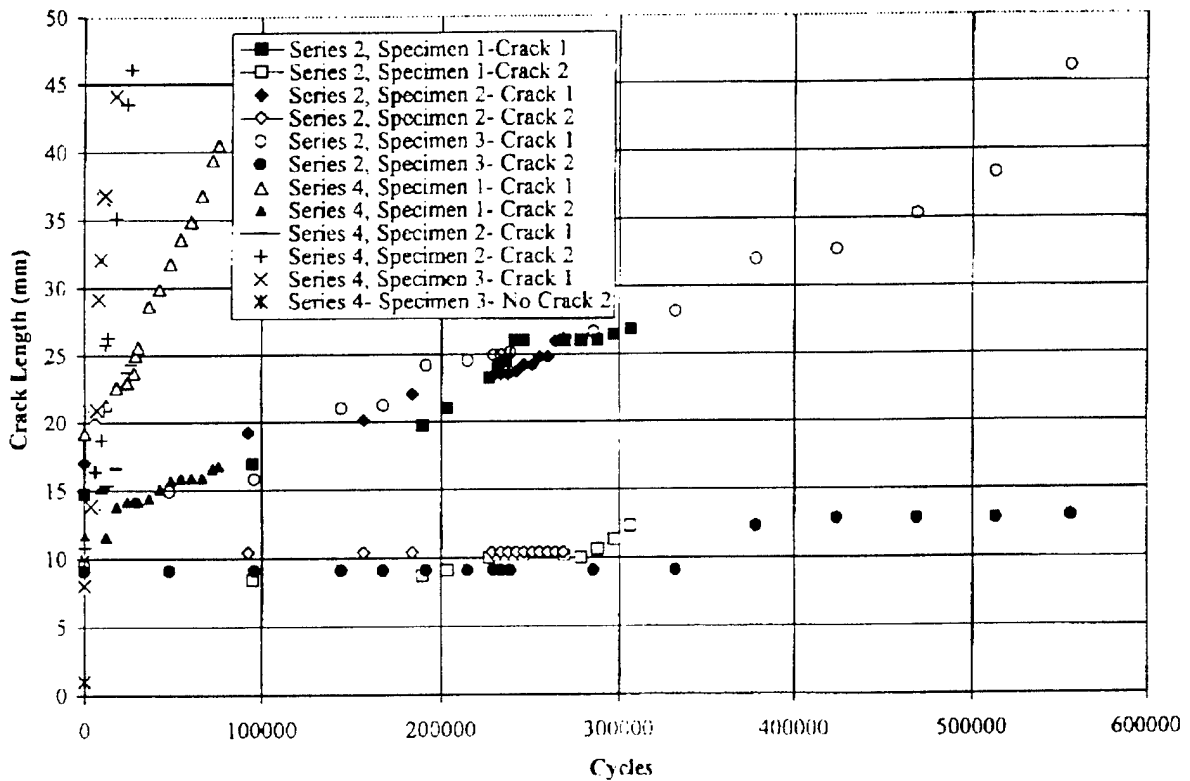


Figure 3.11 Comparison of Crack Growth in Test Series 2 and 4 Specimens (After First Crack Detection)

A comparison of crack growth behavior in Test Series 3 and 4 is shown in Figure 3.12. The specimens in these test series are made from same material and have the same size (Length and Width). However, the thickness of Test Series 4 is three times that of Test Series 3 specimens. The maximum strains in both the specimen series are almost the same. Hence, crack growth behavior is expected to be similar. However, Figure 3.12 indicates the crack growth in Test Series 3 to be much faster as compared to Test Series 4. The test frequencies (resonant frequencies) of two specimen series are different. The resonant frequency of Test Series 4 specimens (82-83 Hz) is 3 times that of Test Series 3 specimens (27-28 Hz). It is pointed out in Reference 14 that higher frequency causes reduction in stress intensity factors, hence, slower crack growth. Also, in thicker specimens under fully reversed bending the cracks may not initiate in the same through-the-thickness plane. Hence, instead of one crack there may be two parallel cracks on each side of specimen centerline shielding each other. This will significantly reduce crack growth rate.

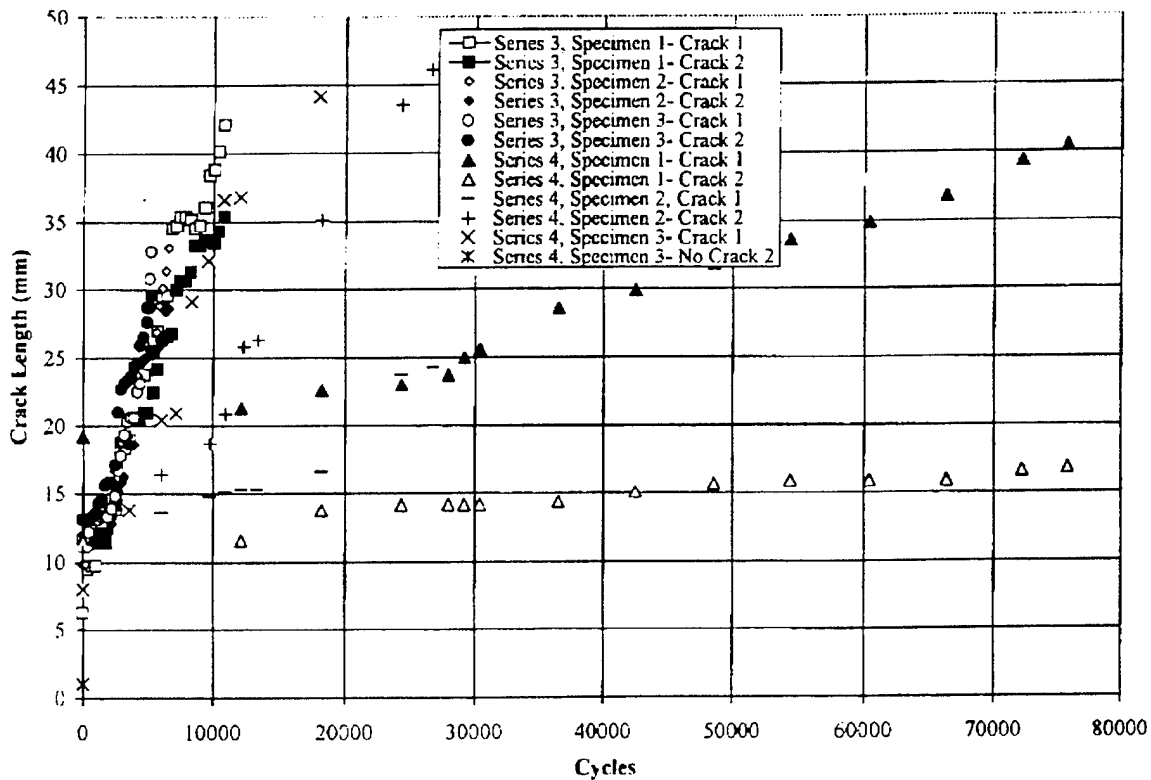


Figure 3.12 Comparison of Crack Growth in Test Series 3 and 4 Specimens (After First Crack Detection)

3.2 Crack Growth Prediction

The review of crack growth data, discussed in Subsection 3.1, indicates that a number of factors need to be considered in making crack growth predictions. The strains and corresponding stresses produced due to vibratory loading (Figure 2.13) are an order of magnitude higher than one would expect from static analysis. Also, the bending moment in the panel varies from zero at free end to maximum value at the support as shown in Figure 2.8b. Current solutions for stress intensity factors, available in literature, are for the case of a constant moment applied to a panel. The use of such a solution to variable applied moment shall be an approximation. Based on literature review of available analyses and test data, the following factors need to be considered for crack growth predictions under acoustic and vibratory loads-

- 1) Dynamic stresses
- 2) Influence of vibratory loads on stress intensity factors
- 3) Interaction between cracks
- 4) Stress intensity factors due to bending loads

- 5) Effect of support conditions
- 6) Influence of dynamic loads on crack initiation
- 7) Crack initiation under bending loads
- 8) Influence of dynamic loads on fracture toughness

Analytical crack growth predictions were made for Test Series 1, 3 and 4. Test Series 2 data could not be analyzed as test data indicated cracks to grow in different through-the-thickness planes on each side of the thick (0.125-inch (3.2-mm)) test specimens. Test Series 4 specimens are also 0.125-inch (3.2-mm) thick specimens, however, one of the specimens showed only one crack growing, hence, data from this specimen was considered valid. AFGROW computer program was used to predict crack growth in test specimens before bonding of repair patches and after bonding of repair patches. In making crack growth predictions with AFGROW, the following analysis cases were considered.

- 1) Use AFGROW computer code with present analytical capabilities.
- 2) Modify AFGROW stress intensity factors (SIFs) to account for the dynamic effects on SIFs. The dynamic effects on SIFs were considered based on the analysis reported in Reference 14.
- 3) Account for the effect of parallel cracks in the test specimens based on analysis of Reference 15. The test data have shown two cracks to grow one on each side of the central load application point (Figure 2.3). Parallel cracks tend to shield each other and thereby reduce SIFs.

3.2.1 Crack Growth Prediction in Panels Without Composite Patch

Comparison of observed and AFGROW predicted crack growth in Test Series 1 specimens is shown in Figure 3.13. The AFGROW predictions are shown for the three analytical cases discussed above. The AFGROW predictions accounting for the dynamic and parallel crack effects agree well with test data initially up to 20-mm crack length. For larger crack lengths, observed crack growth is significantly slower. This is due to the fact that the bending SIF in AFGROW are for the case of plate with a constant far field applied moment. The present case of vibrating plate under consideration is subjected to zero moment at free end and maximum at the fixed end where cracks initiate. The SIF from AFGROW library will give higher value than for actual loading case. The error is likely to be higher for short span panels. The AFGROW analysis needs to be modified for the present bending case.

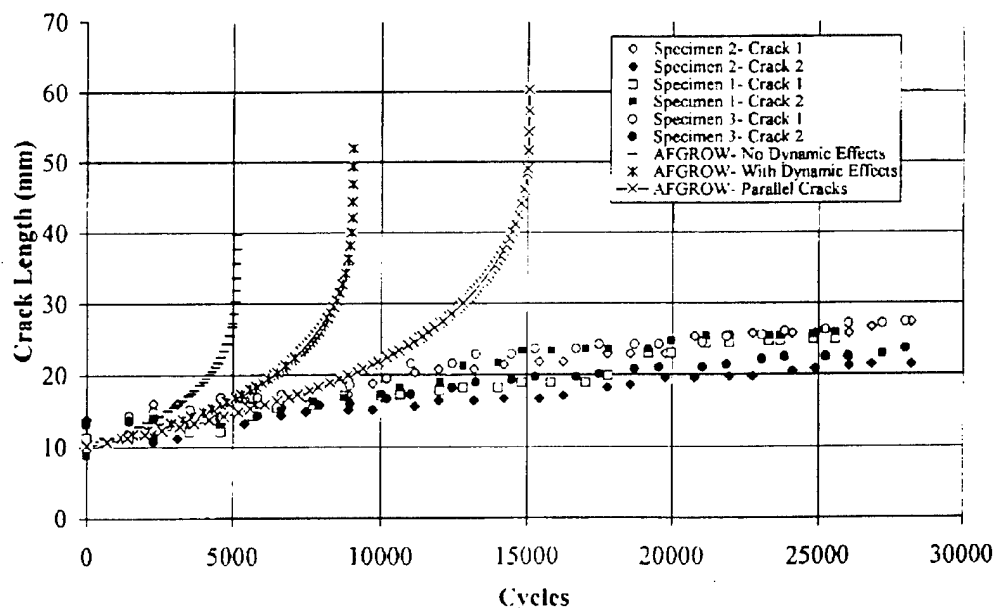


Figure 3.13 Observed and Predicted Crack Growth in Test Series 1 (185x85 mm) 1-mm Thick Specimens (After First Crack Detection)

A comparison of observed and AFGROW predicted crack growth in Test Series 3 specimens is shown in Figure 3.14. The AFGROW predictions are shown for the three analytical cases discussed above. The AFGROW predictions accounting for the dynamic effects agree well with test data initially up to about 30-mm crack length. However, for larger crack lengths observed crack growth is significantly slower. The modified AFGROW predictions accounting for dynamic and parallel crack effects agree well with test data. However, the slowing of crack growth exhibited by the test data is not predicted by analysis. This may be due to the fact that the bending stress intensity factors in AFGROW are for case of plate with constant far field applied moment. In the present case, the vibrating type plate under consideration is subjected to zero moment at free end and maximum moment at fixed end where cracks initiate.

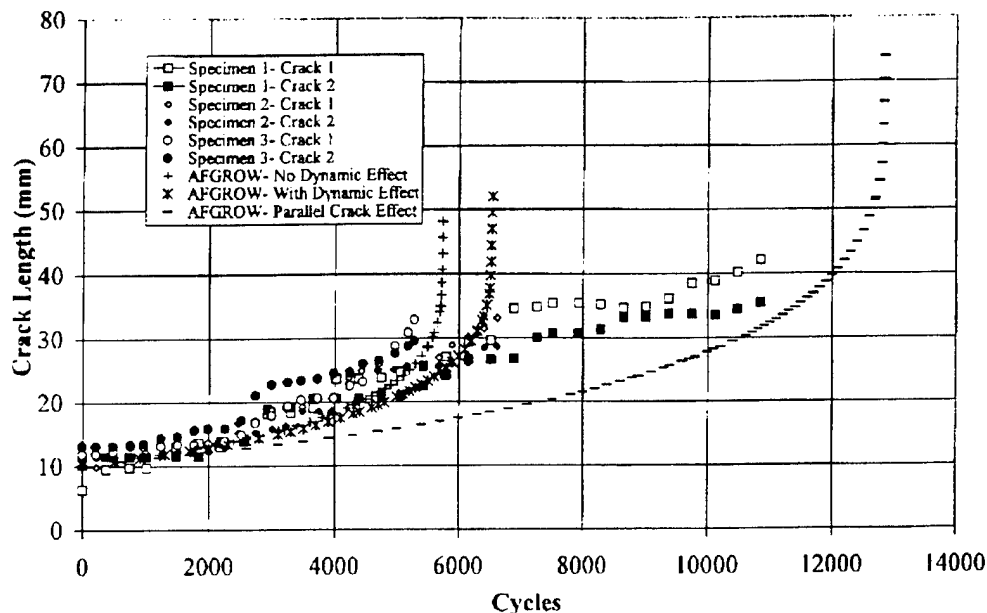


Figure 3.14 Observed and Predicted Crack Growth in Test Series 3 (360x170 mm) 1-mm Thick Specimens (After First Crack Detection)

A comparison of observed crack growth and AFGROW predicted crack growth in Series 4 specimens is shown in Figure 3.15. The AFGROW predictions are shown for the three analytical cases. The AFGROW predictions accounting for dynamic and parallel crack effects under-predict crack growth life. Specimen 3 had only one crack growing and crack growth in this specimen is significantly faster as compared to other specimens. AFGROW predictions show good correlation with test data from this specimen.

3.2.2 Crack Growth Prediction in Panels With Bonded Composite Patch

Crack growth data provided by WPAFB (References 1-4) on test specimens, obtained after bonding of composite patches, were analyzed using AFGROW code. Test data from Test Series 1 and 2 could not be analyzed as the testing was conducted at a variety of stress levels. In these test series, it was not possible to grow cracks after a few million cycles and stress levels were increased to grow the cracks. The input load levels were gradually increased to 10g, 15g and 20g. The initial input load levels prior to bonding of composite patches were 6g. The damage occurred in test specimens at different stress levels and the patch experienced stiffness reduction and strength degradation under the high number of cycles. Hence, AFGROW analysis could not be directly applied to these test series. Test series 3 and 4 specimens were cycled at initial input load level of 3g after bonding of composite patches. AFGROW code was used to predict crack growth in these specimens after composite patches were bonded. The cycles were counted from the time testing was started after bonding of the patches.

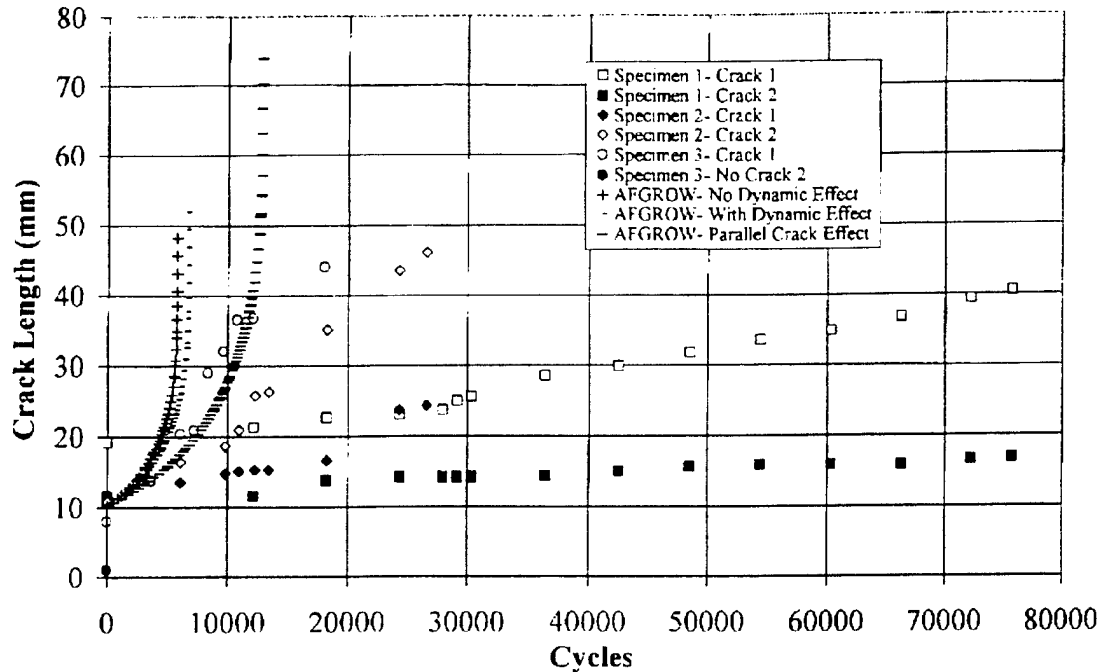


Figure 3.15 Observed and Predicted Crack Growth in Test Series 4 (360x170 mm) 3.2-mm Thick Specimens (After First Crack Detection)

AFGROW code bonded composite patch analysis was used for crack growth predictions. The composite patch stress intensity factors obtained from AFGROW code were modified to account for frequency effects based on Reference 14 analysis, and parallel crack effects based on Reference 15 analysis. Crack growth in Test Series 3 specimens is shown in Figure 3.16 along with AFGROW predictions. AFGROW predictions were made accounting for the effect of dynamic loads, parallel cracks and composite patches on SIFs. The test data shows a large scatter. One specimen shows very short crack growth life. Total crack growth life of other two specimens agrees well with modified AFGROW predictions.

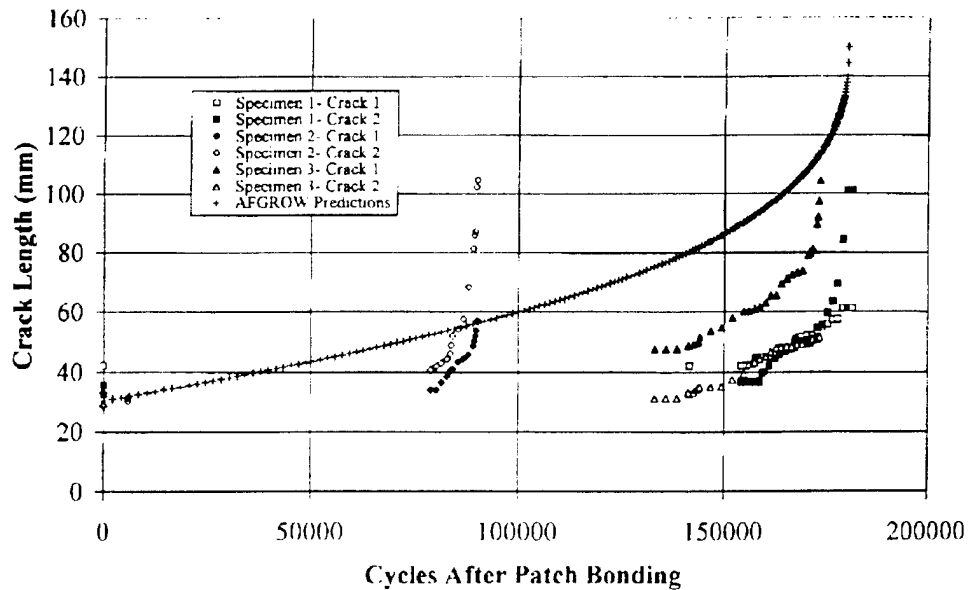


Figure 3.16 Observed and Predicted Crack Growth in Test Series 3 Patched 0.04-inch (1-mm) Thick Specimen (Cycled at 3g)

Crack growth in Test Series 4 specimens is shown in Figure 3.17 along with AFGROW predictions. AFGROW predictions were made accounting for the effect of dynamic loads, parallel cracks, and repair patches. Crack growth test data from one crack of Specimen 1 agrees well with AFGROW predictions. Other cracks show longer crack growth life as compared to AFGROW predictions.

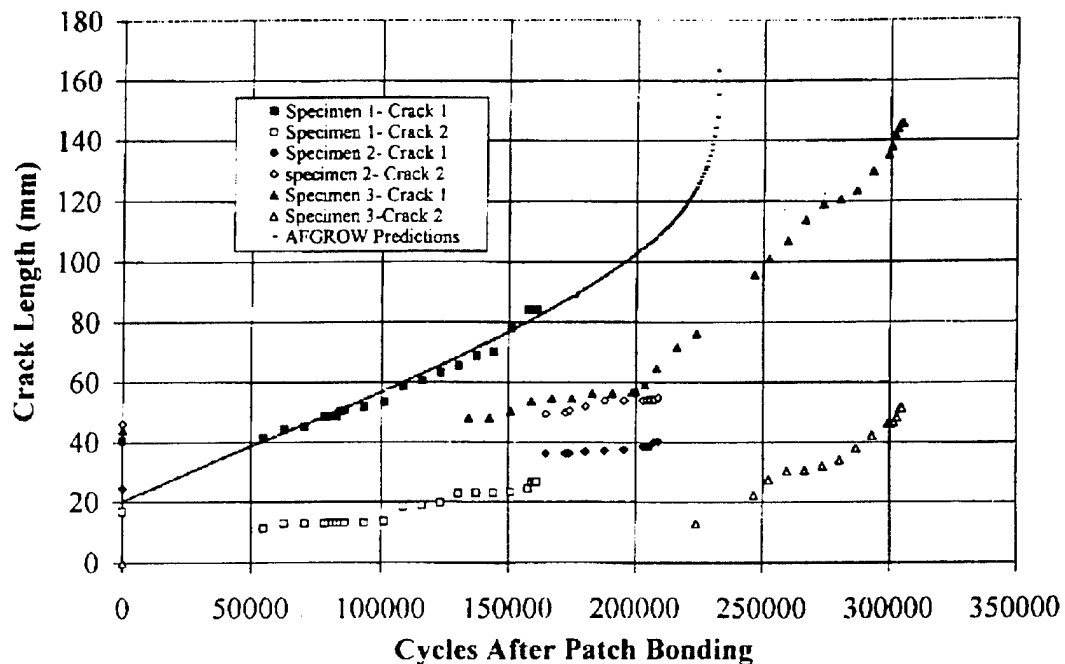


Figure 3.17 Observed and Predicted Crack Growth in Test Series 4 Patched 0.125-inch (3.2-mm) Thick Specimen (Cycled at 3g)

3.3 Assessment of AFGROW Code Capabilities

The correlation between crack growth predictions with AFGROW code and test data on panels tested under vibratory loads indicates that AFGROW code has very good potential to make reliable crack growth predictions for structures subjected to vibratory and acoustic loads. In addition, AFGROW code can be used to design composite patch repairs for structures subjected to vibratory loads. However, the following modifications/developments are required-

1. Dynamic stress analysis of structures
2. Influence of vibratory loads on stress intensity factors
3. Stress intensity factors for panels subjected to variable bending moment along span
4. Effect of support conditions
5. Influence of dynamic loads on fracture toughness
6. Interaction between cracks

The application of current retardation models (e.g., crack closure, Willenborg, etc.) was not investigated in present studies. The effect of dynamic loads on retardation models is not known. The application of these models to dynamic loading needs to be investigated to make predictions under realistic loading conditions.

SECTION 4

VISUAL CRACK MEASUREMENT SYSTEM

A Visual Crack Measurement System (VCMS) using Temperature Sensitive Paint (TSP) has been developed in References 1-2 and is shown in Figure 4.1. The system was used to measure crack growth in specimens with and without bonded composite reinforcement, tested under vibratory loads. However, the crack growth measurements were taken at regular intervals by stopping the test. This VCMS provides an excellent basis for developing an integrated VCMS system that will perform the following functions-

1. Continuously monitor and analyze the crack initiation and growth data in laboratory and field environments.
2. Evaluate structural integrity of structural components subjected to vibratory and acoustic loads
3. Design composite patch repairs for structural component for acoustic and vibratory loading
4. Identify inspection requirements for structures

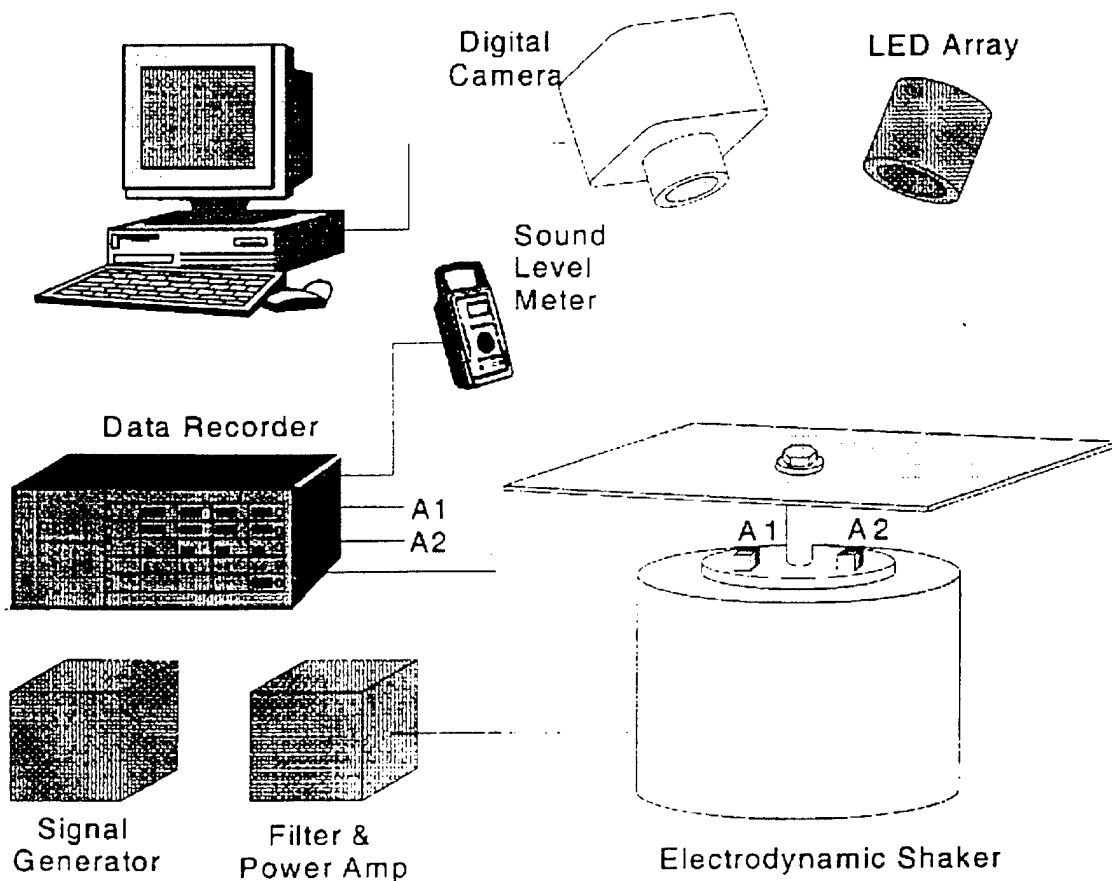
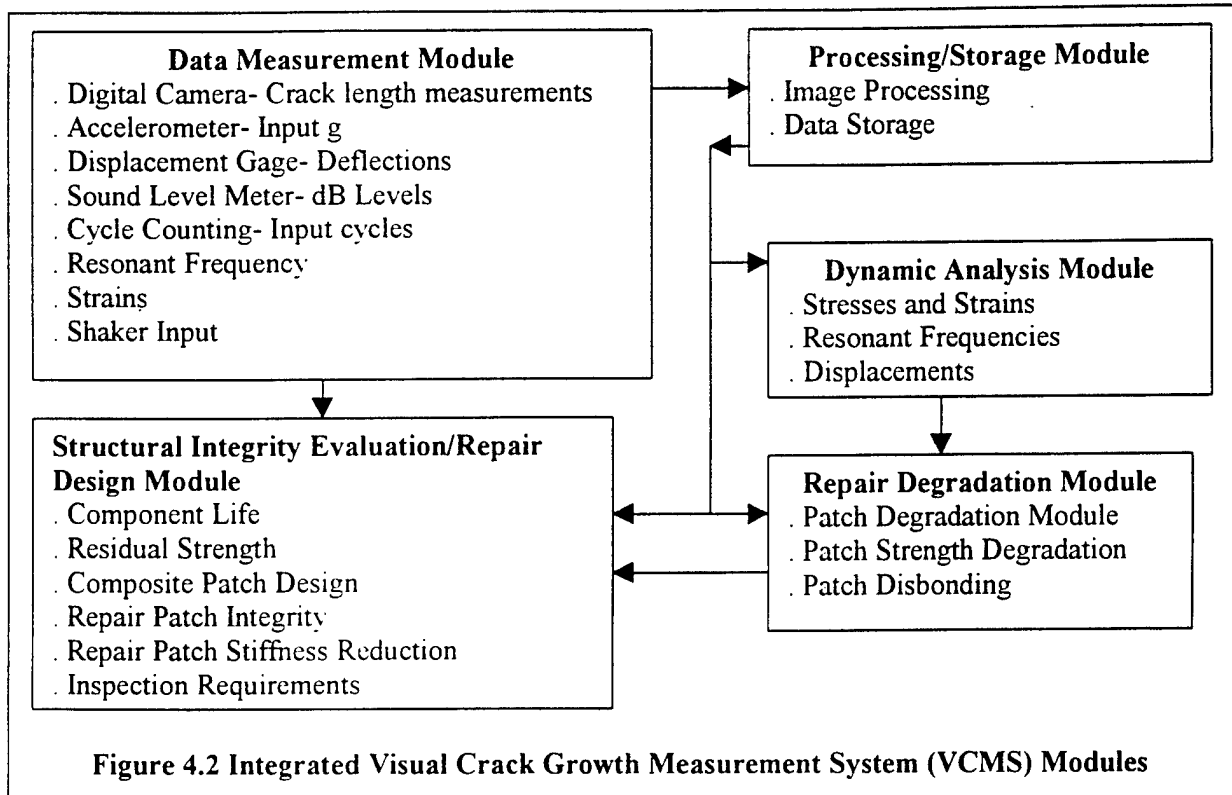


Figure 4.1 Visual Crack Measurement System (VCMS)

Considering the requirements of integrated VCMS, various modules of integrated VCMS have been developed. These modules are shown in Figure 4.2. In its most complete form the system will control the introduction of dynamic loads, simultaneously track multiple transducer outputs (strain gauges, displacement transducers, etc.), and collect and analyze crack images. The system would automatically generate transducer output and cycles versus crack length for the operator. The VCMS design consists of the following basic components:

1. Temperature Sensitive Paint (TSP)

TSP is a luminescent paint providing an opportunity to determine surface temperatures. TSP is excited by the ultraviolet light of 280 to 390 nm spectral range and emits red light of 580 to 630 nm spectral range. Intensity of emitted light decreases with temperature increase. TSP is destroyed at temperatures above 120°C. TSP may be applied by a sprayer to the surfaces of steel, aluminum, wood, composites, and certain types of plastics. In Reference 2, TSP developed by Innovative Scientific Solutions Inc. (ISSI) was successfully used to detect cracks. Hence, ISSI developed TSP is recommended for integrated VCMS.



The TSP technology requires extremely sophisticated image processing techniques. The ISSI developed software called OMS package that is applicable to TSP as well as pressure sensitive paints is suggested. This software program has the following attributes-

- Field- Pressure and temperature field reconstruction, including image resection, filtering, and enhancement.
- Calibration- Temperature and pressure sensitive paint calibration.
- View- Image filtering and restoration

2. Digital Camera with filter and Light Emitting Diode (LED) illumination source with support fixtures.

In References 1-4, a Charged Coupled Device (CCD) Photometric Series 300 digital camera has been used with TSP to detect cracks. The camera is a 16-bit camera. A similar camera as well as a conventional digital camera are recommended. CCD 16-bit cameras are rather expensive, making an integrated VCMS using this type of camera less affordable. In order to reduce the cost of the VCMS, it is desirable to investigate the possibility of using an inexpensive camera such as Sony Mavica Digital. The camera has 3.34 Megapixel CCD image sensor. The cost of the Sony camera is less than one tenth of that for Photometric camera. It is suggested that the pictures shall be taken every 2 seconds with the camera.

An illumination source is required for a VCMS. It is suggested to use ISSI manufactured LM-Series LED source including P2-464 LED Pod, Optical Filter, Diffuser, and Power Supply.

3. A laptop computer and software for hardware control, data collection, analysis and storage
 It is envisioned that all the data collected from the camera and from transducers will be stored in a laptop computer. In addition, the VCMS on laptop computer will have analyses modules including a crack growth prediction code such as AFGROW. The computer shall perform the analyses once testing is completed.

4. Multiple channel analog to digital and digital to analog module
 This module plugs directly into the laptop PC.

5. Transducers (strain gauges, integrated circuit piezoelectric and non-contacting displacement transducers, and accelerometers) and wiring network
 Accelerometers shall be a part of VCMS for on-the-aircraft use at depot level inspections.

6. Shaker and shaker controller

A portable shaker shall be a part of VCMS. The shaker is primarily for on-the-aircraft applications i.e. for exciting panels when inspections for cracks are being made at depot level. For on-the-aircraft depot level inspections, it is necessary to excite aircraft panels after the paint has been applied to the surface to be inspected. A portable shaker will be used to excite the aircraft panels. A portable fixture of the type shown in Figure 4.3 shall be fabricated for mounting the shaker.

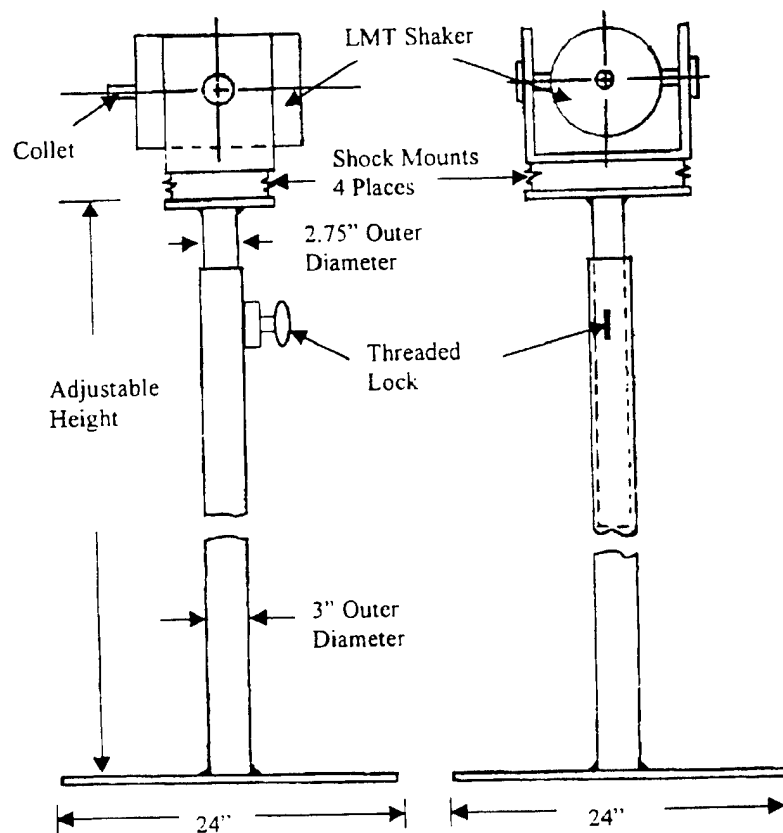


Figure 4.3 Portable Shaker Mounted Assembly

The fixture can be designed to have extension capability to the required height and may be rotated on its trunnion base. A small (0.5- to 0.75-inch diameter) adjustable length tube will connect the shaker collet to a suction cup. The suction cup will be used to excite aircraft panel. A small portable vacuum pump shall

be used to provide vacuum for the suction cup. The shaker can also be used for laboratory testing of specimens. The shaker shall have capability for sinusoidal as well as random excitation.

An operators manual shall be required for VCMS. The projected output parameters of an integrated VCMS are shown in Figure 4.4

- Component Life
- Component Residual Strength
- Resonant Frequencies
- Repair Patch Design
 - Material (composite, adhesive, damping)
 - Size
 - Repair Patch Lay-up
- Repair Patch Stiffness Loss
- Repair Patch Disbonding
- Recommended Testing
 - Equipment
 - Test Procedures
 - Temperature Sensitive Paint Applications
- Inspection Requirements

Figure 4.4 VCMS Output Parameters

SECTION 5

SUMMARY AND ASSESSMENT OF TECHNICAL MERIT

5.1 Summary

Analyses techniques have been developed to compute resonant frequencies of metallic panels subjected to vibratory loads produced by shaker excitation. The analyses have been developed for the following cases-

1. Panels with no cracks
2. Panels with cracks
3. Panels with cracks and bonded composite patches

For cases 1 and 2 closed form solutions were obtained. For case 3 a FORTRAN software program is written to compute resonant frequencies of cracked panels with bonded repair patches. The computer program is operational on a PC and computer run time is a few seconds.

The analyses were verified with available test data generated at AFRL, Wright Patterson Air Force Base (WPAFB), Ohio. A good agreement was obtained between predicted and test resonant frequencies.

Mathematical stress analysis techniques were developed for panels subjected to vibratory loads produced by shaker excitation. Closed form solutions were obtained. The analysis method was verified with the test data provided by AFRL/WPAFB. The results of predicted strains agreed well with strains obtained by the Air Force from measured deflections and beam theory.

Crack growth data generated by AFRL/WPAFB on aluminum panels with and without bonded repair patches under vibratory loads in a shaker were reviewed. The trends in crack growth data were identified. The application of the crack growth computer code AFGROW to predict crack growth in panels subjected to vibratory loads was evaluated. It was determined that the stress intensity factor library in AFGROW code needs to be modified to account for the following factors-

1. Dynamic stresses
2. Influence of vibratory loads on stress intensity factors
3. Interaction between cracks
4. Stress intensity factors due to bending loads
5. Effect of support conditions
6. Influence of dynamic loads on crack initiation
7. Crack initiation under bending loads
8. Influence of dynamic loads on fracture toughness

The stress intensity factors in AFGROW code were modified to account for dynamic stresses, frequency effects, and crack interaction effects. AFGROW code with modified stress intensity factors was used to predict crack growth lives of panels with and without bonded patches. The predicted crack growth lives showed good agreement with test data. Stress intensity factors (SIFs) due to bending loads in AFGROW library need to be modified for variable applied moment loading cases. None of the existing crack growth codes have stress intensity factors for such loading conditions. Also, literature search did not show any solutions for such loading cases. The finite element technique may have to be used to obtain SIFs.

Design requirements and various functions to be performed by an integrated Visual Crack Measurement System (VCMS) have been defined. Various modules and their functions were also identified. Various components of the system were established. The integrated VCMS design is modular to perform the following functions-

1. Continuously monitor and analyze the crack initiation and growth data in laboratory and field environments.
2. Evaluate structural integrity of structural components subjected to vibratory and acoustic loads.
3. Design composite repairs for structural components subjected to acoustic and vibratory loading.
4. Identify inspection requirements for structures.

The possibility of using the system on an actual aircraft for crack detection was explored. The design of a portable shaker system to excite aircraft panels in the field was developed.

5.2 Assessment of Technical Merit

Phase I objectives have been fully achieved. Analytical tools have been developed to predict resonant frequencies of panels with and without cracks. Analytical techniques to predict resonant frequencies and stresses have also been developed for panels with cracks and bonded patches. In addition, a PC based FORTRAN code was written to obtain resonant frequencies of panels with bonded patches in fixed-free mode vibration conditions. The analytical predictions have shown good agreement with available test data. Dynamic stress analysis was developed for panels with base excitation. Predicted strains agreed well with test data.

Potential application of AFGROW code to predict crack growth in panels with and without bonded patches under vibratory loads was evaluated. It was shown that AFGROW code has a very good potential to predict crack growth under vibratory loads. However, some modifications need to be made in the stress intensity factors library in AFGROW code. It was shown that composite patch analysis in AFGROW code could be extended to vibratory loads with some modifications. The modifications required in AFGROW were identified.

The functions to be performed by an integrated Visual Crack Measurement System (VCMS) were identified. Various requirements and modules of VCMS were established. Elements of VCMS and their functions were defined.

The analytical techniques to obtain resonant frequencies, developed in Phase I, can be extended to other panel geometries. AFGROW computer code with suggested modifications could be used to evaluate structural integrity of aircraft structures subjected to acoustic and vibratory loads. The code can also be extended to design composite patch repairs for structures subjected to dynamic loading conditions. These modifications to AFGROW code are planned for Phase II program. Phase II program when completed shall develop an integrated VCMS capable of the following functions-

1. Detect cracks in specimens being tested under vibratory loading in laboratory.
2. Detect cracks in aircraft structures subjected to in-service vibratory loads. The inspection of aircraft will be done at depot level with a portable unit.
3. The software in the system shall have capability to evaluate structural integrity of components subjected to acoustic or vibratory loading. The structural integrity can be evaluated in real time when the damage is detected if the information on loads spectrum experienced by a component is previously stored in the computer. The loads information on various aircraft can be stored in the VCMS system.
4. The knowledge-based software in the system can design composite patch repairs for components subjected to acoustic or vibratory loads. The software shall recommend repair materials, processes, and repair design. In addition, the software shall predict repair design life, and inspection requirements.
5. Engineers in design offices as well as repair centers can use the software part of the VCMS, thereby expediting a rapid design and installation of patch repairs.

SECCION 6

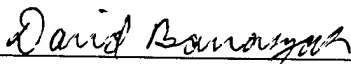
REFERENCES

1. Banaszak D, Lassiter J. O and Baust H. D, "Thermal-Optical Measurements in Structures with Damped Composite Repairs", The USAF Aircraft Structural Integrity Programs Conference December 1999.
2. Banaszak D, Dale G. A, Watkins N. and Jordan J. D. "An Optical Technique for Detecting Fatigue Cracks in Aerospace Structures", 18th International Congress on Instrumentation in Aerospace Simulation, Toulouse, France, June 1999.
3. Banaszak D and Dale G. A, "Two-Level Factorial Experiment for Crack Length Measurements of 2024-T3 Aluminum Plates Using Temperature Sensitive Paint and Electrodynamics Shakers", Proceeding of the Section on Physical and Engineering Sciences, American Statistical Association, August 1999.
4. Banaszak D, Dale G. A and Baust D. J, "Effectiveness of Damped Fiberglass Patches on Vibrating 2024-T3 Plates", Proceedings of SAMPE 2001 Conference, Long Beach California, May 2001.
5. Heimerdinger M, Ratwani M. M. and Ratwani N. M. "Influence of Composite Repair Patch Dimensions on Crack Growth Life of Cracked Metallic Structures", Proceedings of Third FAA/DoD/NASA Conference on Aging Aircraft, Albuquerque, New Mexico, September 1999.
6. Helbling J, Grover R and Ratwani M.M "Analysis and Structural Test of Composite Reinforcement to Extend the Life of T-38 Lower Wing Skin", Proceedings Aircraft Structural Integrity Conference, San Antonio, 1998.
7. Helbling J, Heimerdinger M and Ratwani M.M. "Composite Patch Repair Applications to T-38 Lower Wing Skin", Proceedings of Second NASA/FAA/DoD Conference on Aging Aircraft, Williamsburg, Virginia, 1998.
8. Helbling J, Ratwani M. M and Heimerdinger M. "Analysis, Design and Test Verification of Composite Reinforcement for Multi-site Damage", Proceedings of 20 International Conference on Aeronautical Fatigue Symposium, Seattle, Washington, 1999.
9. Ligoure Salvatore, Hunter Kipplan, Perez Rigoberto and Beier Theodore, "Flight Test Evaluation of Damped Composite Repairs for Sonic Fatigue", 40th AIAA/ASME/ASCE/AHS/ASC Structures, Structural Dynamics, and Materials Conference, St. Louis, April 1999.
10. Schubbe Joel J, "Thickness Effects on a Cracked Aluminum Plate with Composite Patch Repair", AFIT/DS/ENY/97-4, 1997.
11. Meirovitch L, "Analytical Methods in Vibrations", Published by Macmillan Company, New York, 1967.
12. Young D and Felgar R. P. "Tables of Characteristic Functions Representing Normal Modes of Vibration of a Beam", The University of Texas Publication, Engineering Research Series No. 44, 1949.
13. Richards E. J and Mead D. J. "Noise and Acoustic Fatigue in Aeronautics", Published by John Wiley and Sons.
14. Folias E. S. "On the Steady State Transverse Vibrations of a Cracked Plate", Engineering Fracture Mechanics, 1968.
15. Ratwani M. M. "Wechselwirkung von Rissen (Interaction Between Cracks)" Institut fur Festkorpermechanik Research Report No. 5/72, Freiburg, West Germany, 1972.


NOTICE

Using government drawings, specifications, or other data included in this document for any purpose other than government procurement does not in any way obligate the U.S. Government. The fact that the government formulated or supplied the drawings, specifications, or other data does not license the holder or any other person or corporation; or convey and rights or permission to manufacture, use, or sell any patented invention that may relate to them.

This technical report has been reviewed and is approved for publication.



David L. Banaszak, Project Engineer
Analytical Structural Mechanics Branch
Structures Division



Daniel B. Shrage, Capt, USAF
Chief, Analytical Structural Mechanics Branch
Structures Division



Jeffrey S. Turcotte, Lt Col, USAF
Deputy Chief, Structures Division
Air Vehicles Directorate

Copies of this report should not be returned unless return is required by security considerations, contractual obligations, or notice on a specific document.